Climatological analysis of seeing conditions at the site of the European Southern Observatory (ESO) in Paranal, Chile

Paula Casals and Martin Beniston

Department of Geosciences
University of Fribourg
Switzerland

Final Report, August 2001

Contract Nr.: 61243 / ODG / 00 / 8543 / GWI / LET

Table of contents

1. Introduction

Prior to setting up its Very Large Telescope (VLT) in Chile, ESO undertook a multi-year climatological assessment of the Paranal site in terms of its suitability for astronomical observations (cloudiness, atmospheric turbidity, thermal turbulence, etc.). Following the construction and start of operations of ESO's VLT in 1998, atmospheric conditions have been considerably different from those observed during the measurement period earlier in the 1990s.

These shifts in climatic patterns, which reduce seeing conditions by as much as 15%, pose the following questions:

- Are the current weather patterns part of a cycle which have already occurred in the past but which was not observed in the mid-1990 ?
- Are they related to ENSO events ?
- Are they totally anomalous and related to global warming ?

Answers to these questions may provide insight into the future prospects for astronomical observations. Furthermore, the methodologies developed here to address these issues may be incorporated as part of an integrated strategy aimed at selecting a new site for ESO's future 100-m telescope.

This report thus attempts to answer these questions based on data analysis. Because the time-series at the ESO site are too short for any meaningful climatological statistics to be compiled, a first step in this research has been to obtain additional observational data from other sites in order to check the consistency between longer-term records and the 15-year ESO data set. Extending the data record provides key answers to whether the current weather patterns are anomalous or not.

Analysis from the NCAR-NCEP (National Center for Atmospheric Research/National Centers for Environmental Prediction) data also provides a synoptic overview to explain shifts in climatic conditions at Paranal. Such shifts include the circulation patterns which can favor or perturb the duration of astronomical observing periods.

Finally, it has been of interest to see to what extent decadal-to-century scale warming has taken place during the 20th Century in northern Chile. This is to ascertain whether global warming is a new factor in the currently-observed weather patterns, or whether the ENSO cycles are the dominant features which determine seeing conditions at the VLT site.

2. A brief review of ENSO

Because many of the processes to be discussed in this report are intimately linked to the ENSO phenomenon, it is worth providing a brief overview of the phenomenon in order to guide the reader in later parts of this report.

The so-called El Niño/Southern Oscillation (ENSO) represents an interplay of coupled ocean-atmosphere phenomena. El Niño is the warm phase of ENSO, in which a weakening of the prevailing easterly Trade winds in the equatorial Pacific allows the eastward propagation of warm waters which normally accumulate to the west of the Pacific basin. Associated areas of deep convection "migrate" eastwards, tracking the propagation of the warm waters which are the principal energy source for convection. The area of anomalously warm waters at the peak of an El Niño episode can reach 30 million km^2, roughly 3 times the size of Canada, and as a consequence the sensible and latent heat exchange at the ocean-atmosphere interface is sufficient to perturb climatic patterns globally. This perturbation occurs in three simultaneous steps:

- vertical transfer of energy, heat and moisture through the deep convection
- horizontal propagation through atmospheric flows at high elevations
- an "overflow" into the mid-latitude synoptic systems which can reinforce or weaken surface pressure patterns and deflect the jet streams from their normal trajectories.

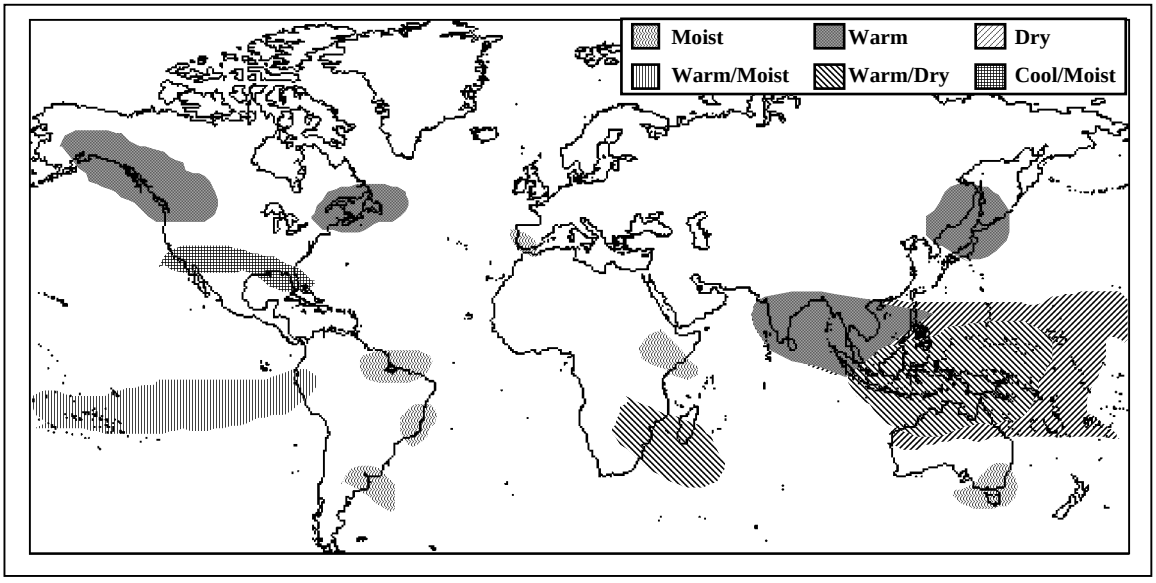

Figure 1: Typical climatic anomalies associated with an El Niño event

Figure 1 illustrates the characteristic climatic anomalies that are driven by El Niño in different parts of the world. It is to be noted that a region of warm and moist air is located in the southern

equatorial Pacific ocean, off the coast of Ecuador and Peru and stretching far eastwards into the Pacific. Any flows from a north-westerly direction would thus be capable of advecting some of this moisture toward northern Chile.

The cold phase of ENSO, commonly referred to as La Niña, occurs sometimes (but not always) at the end of an El Niño event. Anomalously cold waters invade the tropical Pacific region, and the strength of La Niña can in some instances reverse the previously discussed anomaly patterns, i.e., by enhancing respective precipitation or drought patterns where these normally occur.

There is speculation (Wolter and Timlin, 1998) that global warming may enhance the frequency and intensity of ENSO events. This is based on the observation that since the early 1970s, the return period of the warm phase of ENSO has substantially increased. Furthermore, following the 1992-93 event, the waters of the equatorial Pacific did not return to normal conditions for a number of years. Although this may be unrelated to observed warming and could be explained by the chaotic behavior of ocean-atmosphere coupling, if a warmer climate were to be accompanied by increases in El Niño events, then the perturbations to astronomical observations could occur more frequently than currently. The 1997-98 El Niño was the most intense event of the 20th Century, resulting in massive forest fires from Indonesia to Australia, catastrophic flooding in southern and central California, Peru and Chile, crop failures in the Philippines, Indonesia, Brazil and southern Africa. It coincides with the warmest period of the century, lending some credibility to the speculation that there may be a link between global warming and increases in El Niño events. The recent sequence of El Niño episodes have contributed significantly to the increase in global mean temperatures in the 1990s.

3. Observational data

3.1 Data available at Paranal

Cerro Paranal is located at 24°40'S and 70°25'W at 2635 m altitude above sea-level. The time-series of available data span the range 1985-present with, however, some gaps in the series as a result of occasional technical problems. Table 1 provides an overview of the available data at the Paranal site.

The data has been recorded every 20 minutes for each of these parameters. On the basis of this information, monthly-means have been computed for the available time periods. In 1992, in particular, data is missing because observations were suspended at the start of the construction of the ESO Very Large Telescope (VLT).

Parameter	Measurement height	Start	End
Wind velocity (m/s)	10 m	Jan 1985	Dec 2000
Wind direction (°)	10 m	Jan 1985	Dec 2000
Relative humidity (%)	2 m	Jan 1985	Dec 2000
Temperature (°C)	2 m	Jan 1985	Dec 2000
Pressure (hPa)	2 m	Jan 1985	Dec 2000
Dew-point temperature	2 m	Jan 1985	Dec 2000

Table 1: Available climatic data at Paranal

Table 2 shows the optical measurements which are available as monthly means of photometric nights and visibility data (seeing).

Parameter	Description	Start	End
Photometric night fraction	Ratio of number of nights of observations to total number of nights	Sep 1983	Dec 2000
Seeing (arcsec at 0.5 mμ, zenith)	Apparent deformation of the source due to atmospheric transmission	Apr 1987	Feb 2001

Table 2: Available astronomical data available at Paranal

3.2 Data available at Antofagasta

The mean monthly temperature data have been recorded at Antofagasta, located at 23°43'S, 70°43'W and at 135 m above sea level. The upper-air sounding station of Antofagasta is operated by the Chilean Weather Service (Dirección Meteorológica de Chile). Sea-Surface Temperatures (SST) measurements have been recorded off the coast of Antofagasta at 23°39'S and 70°25'W.

Parameter	Start	End
Mean monthly temperature (°C)	Jan 1951	Sep 2000
Mean monthly wind speed at 700 mb (m/s)	Jan 1987	Jun 2000
Mean monthly wind speed at 200 mb (m/s)	Jan 1987	Jun 2000
Mean monthly SST (°C)	Jan 1946	May 1998

Table 3: Available climatic data at Antofagasta

3.3. Other available data

The monthly-mean values of the Southern Oscillation Index (SOI) of the Climate and Global Dynamics division of the University Corporation for Atmospheric Research (CGD/UCAR) and the reanalysis data of the National Centers for Atmospheric Research/National Center for Atmospheric Research (NCEP/NCAR) have also been used for the present analyses. The

NCEP/NCAR data has been analyzed by using the GrADS (Grid Analysis and Display System), a software package which is available on-line for handling the formats of the NCEP/NCAR data.

The SOI data is available on-line from the Climate and Global Dynamics Division of the University Corporation for Atmospheric Research (CGD/UCAR) at URL: http://www.cgd.ucar.edu/cas/climind/soi.html. The SOI is the standard sea-level pressure anomaly between Darwin and Tahiti. Data is available at this site from January 1951 to December 2000. The NCEP/NCAR data is available on-line from the site of the Climate Diagnostics Center of the National Oceanic and Atmospheric Administration (NOAA/CDC) at URL: http://www.cdc.noaa.gov/cdc/data.nmc.reanalysis.html. Much of the data is available as monthly-means at each of the 17 standard pressure levels. Table 4 summarizes the available variables used in the present report.

Parameter (monthly mean values)	**Level**	**Start**	**End**
Geopotential height (m)	700 hPa	Jan 1948	Mar 2001
Wind speed (m/s)	700 hPa	Jan 1948	Apr 2001
Relative humidity (%)	700 hPa	Jan 1948	Apr 2001
Cloud forcing net longwave flux (W/m^2)	Surface	Jan 1948	Apr 2001
SST (°C)	Surface	Nov 1981	Mar 2001

Table 4: Summary of NCEP/NCAR reanalysis data used in this study

4. Climatological analysis of the available data

As a first step, a systematic control of the quality of data was undertaken in order to detect errors or missing data in the Paranal time series; following this, monthly means were computed for the selected variables used in the analyses, namely temperature, wind speed, pressure, photometric nights, and seeing conditions.

4.1. Temperature time series at Paranal

The time series of temperature has gaps in the data between June and October 1987. Mean temperature for the entire period of the record (1985-2000) is 12.7°C. There is a seasonal cycle to temperature, event at these low latitudes and high altitudes, with the lowest temperature of 7.9°C recorded in September 1989, and the highest (17.1°C in January 1998) corresponds to the peak of the 1997-98 El Niño event. The rapid transition to La Niña conditions is highlighted by the drop in temperatures to around 10°C in August 1998. During the southern summers of 1998-99 and 1999-2000, temperatures were systematically lower than in preceding years, with mean temperatures in the 12-13°C range. Southern winters in 1999 and 2000 were also marginally cooler than in previous years, as a result of the long and persistent La Niña event. It is only

towards the end of 2000 that temperatures began to rise once more to levels closer to average conditions (14.1°C).

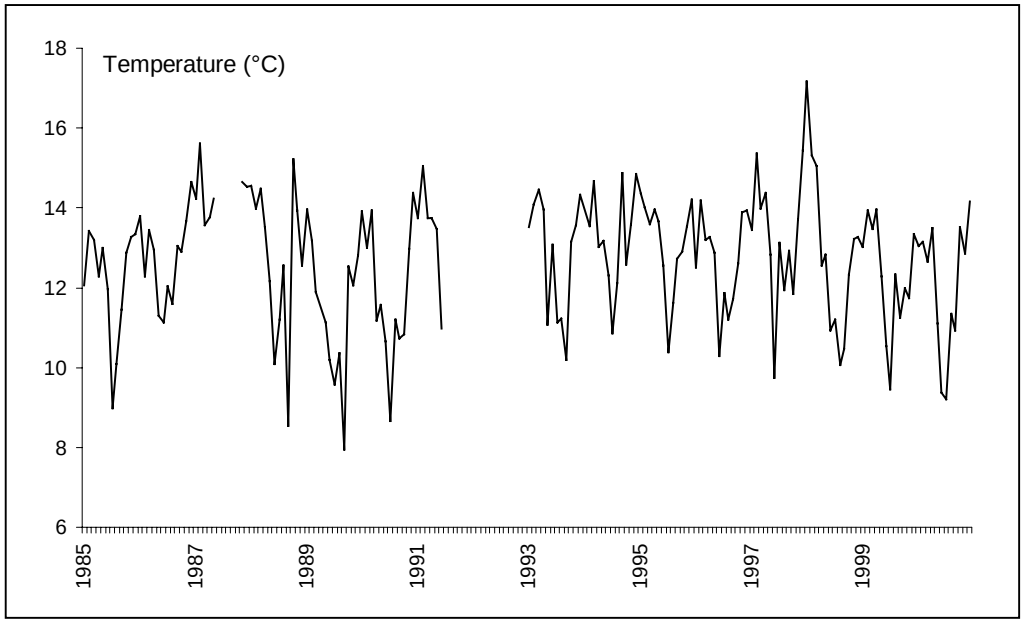

Figure 2: Monthly-mean time series of temperature at Paranal

4.2 Relative humidity at Paranal

Mean relative humidity at Paranal for the 14 years of records is 15.2%, with the lowest values occurring between April and November (3-12%) and the highest during the southern summer (16-44%). In the Paranal series, the months of March 1985, February 1989, January 1997, February 1999, and January 2000 exhibit the highest values of moisture, ranging from 35-44%. Since January 1997 and through 2000, an increase in relative humidity is observed especially during the first three months of the year, as seen in Table 5.

	January	**February**	**March**
1997	38.4	23.4	28.6
1998	20.3	39.2	26.5
1999	22.8	40.0	32.9
2000	44.1	33.5	42.0

Table 5: Monthly-mean relative humidity at Paranal for the first three months of the year from 1997-2000

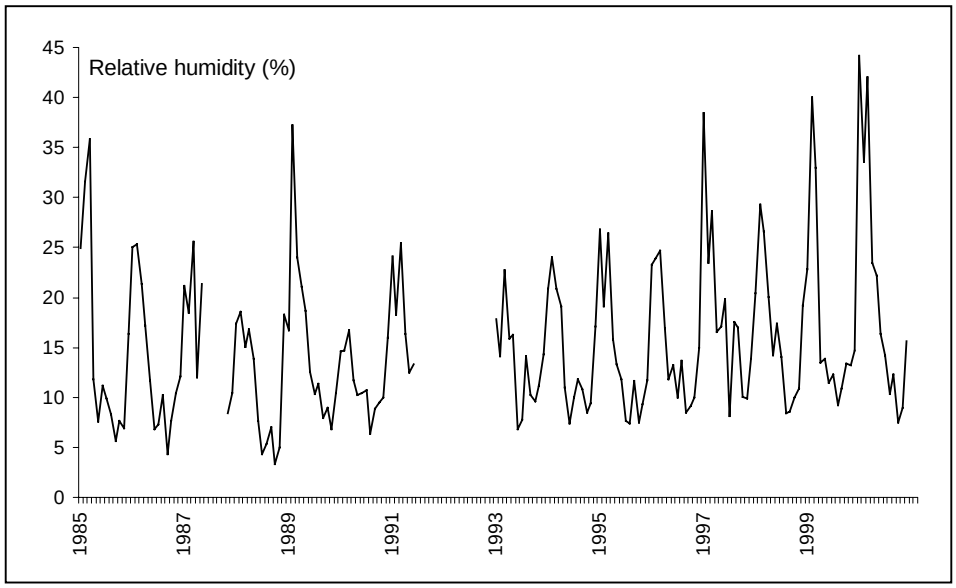

Figure 3: Monthly-mean time series of relative humidity at Paranal

4.3. Pressure at Paranal

The pressure time series of Paranal is one of the most incomplete in the record. Data is missing for the years 1985, 1987, 1988, 1991, 1992 and September 2000. Mean pressure at Paranal for the observational period is 743 hPa. Four years exhibit rather low pressure: 739.4 hPa (November 1986), 739.1 hPa (September 1989), 741.0 hPa (September 1993) and 739.7 hPa (April 1998). Maximum pressures range from 744.1 hPa-744.4 hPa, with the highest on record being 745.2 hPa (February 1991) and 744.6 hPa (May 1991). In February 1998, pressure was 744.4 hPa and fell to 739.7 hPa in April of the same year, to rise again the following month to 744.3 hPa. Problems with the pressure sensor installed prior to 1988 may explain the anomalously low value seen here (Sarazin, 2001, personal communication).

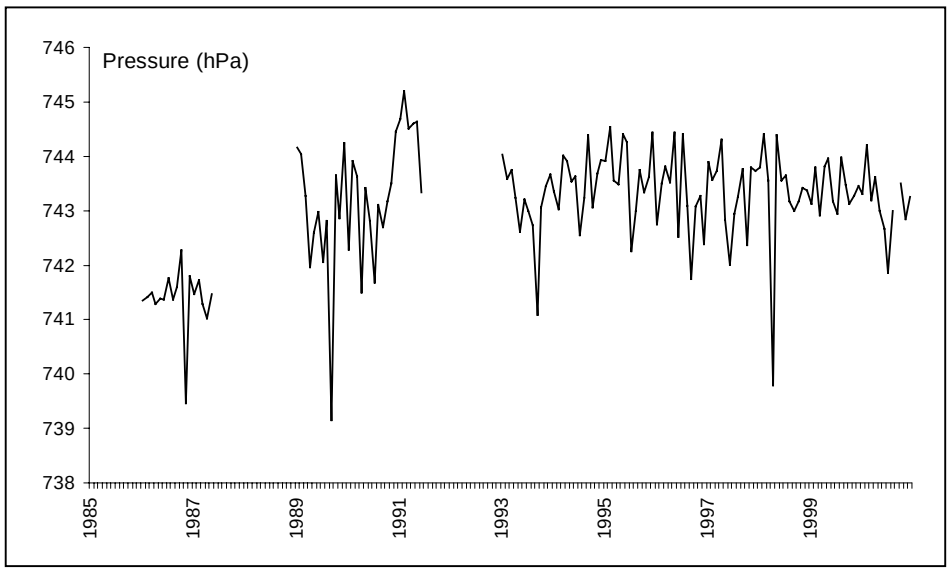

Figure 4: Monthly-mean time series of pressure at Paranal.

4.4. Wind speed at Paranal

It is observed that the strongest wind speeds occur essentially during the southern winter months. The mean wind-speed at Paranal for the observational record is 7.4 m/s, with four types of behavior around this mean. The first type of behavior occurs between January 1985 and May 1987, when wind velocities rarely drop below 6 m/s and seldom exceed 9 m/s. The second set is observed between November 1987 and ends in June 1991. Here, wind velocities exceed 9 m/s and even 10 m/s on 5 occasions during this period, all during the southern winter or spring. From January 1994 to May 1996, the range of velocities is lower, from a minimum of 4.5 m/s to a maximum of 8.8 m/s. The last set begins in June 1996 and ends in December 2000, with the highest systematic wind velocities recorded during the 1985-2000 period, but also some of the lowest minimum wind speeds. The variability of wind is thus greatest in the last part of the record, compared to the preceding decade. In order to accommodate the infrastructure of the telescope, it was necessary to cut off 36 m off the summit, which consequently resulted in a lowering of wind velocity through a reduction in the Venturi effect (Sarazin, 2001, personal communication).

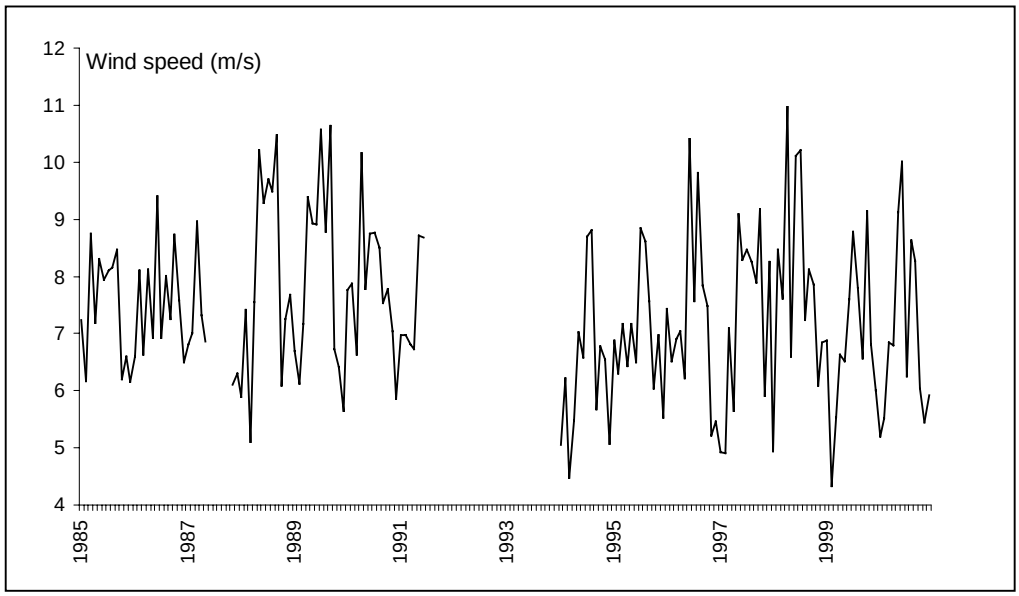

Figure 5: Monthly-mean time series of wind speed at Paranal

4.5. Fraction of photometric nights at Paranal

A photometric night is defined as a situation where skies are cloud-free up to 18° above the horizon for at least six consecutive hours. The fraction of photometric nights is the ratio of photometric nights to the total number of nights in a given month. The average photometric night fraction for the entire period of observation is 0.77. Four distinct situations arise from 1983 to December 2000, as seen in Figure 6. The first occurs between September 1983 through March 1989. During this period, 5 months are entirely cloud-free for at least six consecutive hours (photometric night fraction: 1), with only one value below 0.6 (0.55 in October 1984). Other than

these extremes, the range of photometric night fractions is between 0.60 and 0.94. The second period spans the period from March 1989 through December 1992. During this part of the series, the range is from 0.45-0.93, with only one month where a value of the photometric night fraction exceeds 0.90. The third period of the record stretches from December 1992 to May 1997, with a large number of months with photometric night fractions in excess of 0.90; October 1994 and January 1996 reach the optimal value of 1. The last part of the series runs from May 1997 to December 2000, and behaves in much the same way as the second period (1989-1992). Highest photometric night fractions are in the range 0.90-0.94, and the lowermost fractions fluctuate between 0.41 and 0.60; there is thus an obvious reduction in astronomical observation periods compared to the 1992-1997 period and which, unfortunately, corresponds to the first years of operation of the ESO VLT.

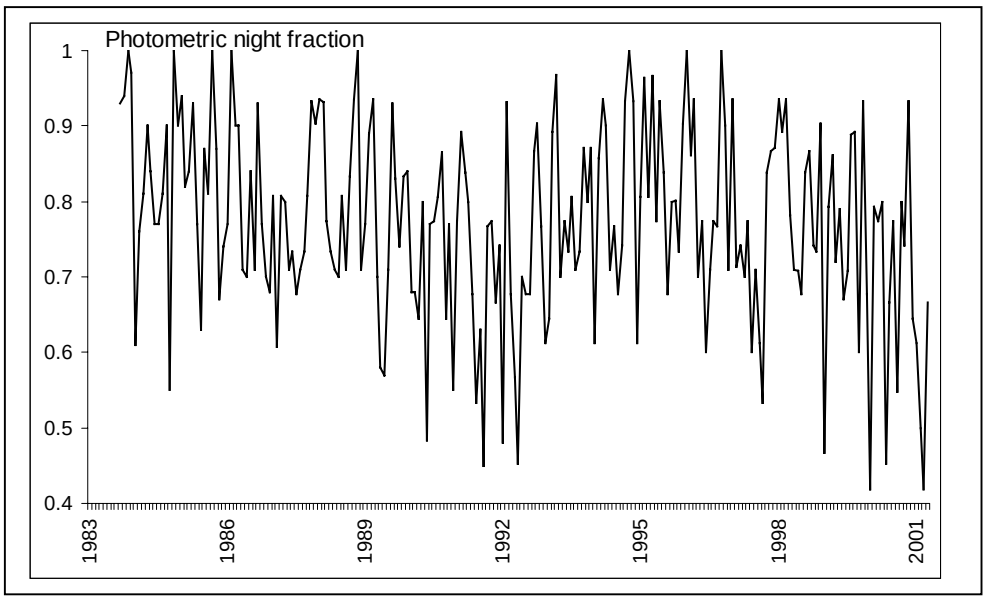

Figure 6: Monthly-mean time series of photometric night fraction at Paranal

4.6. Visibility conditions ("seeing") at Paranal (arcsec at 0.5μm zenith)

"Seeing" is the term astronomers use to describe the sky's atmospheric conditions. The atmosphere is in continual motion with changing temperatures, air currents and turbulence, weather fronts and dust particles. These factors cause the star images to shimmer (twinkle). If the stars are twinkling considerably, seeing conditions are "poor", and the reverse is true when the star images are steady. On deep sky objects, the most important factor is the transparency of the atmosphere. This is a measure of how dark the sky is on a given night, determined by clouds, dust, haze and light pollution. An indication of the seeing is invaluable in comparing observations with those made on other occasions. The effects of poor seeing upon visual observation are, principally, small and erratic movements of the object and diffusion of its image.

At the Paranal site, there are several sets of missing data in the time series of seeing. The mean seeing conditions have been computed for the period between April 1987 and August 1998, and the mean value is 0.7. Table 6 highlights the periods in which seeing is close to the mean, or above or below 0.7.

	Jan	Feb	Mar	Apr	May	Jun	July	Aug	Sep	Oct	Nov	Dec
1987												
1988												
1989												
1990												
1991												
1992												
1993												
1994												
1995												
1996												
1997												
1998												
1999												
2000												
2001												

Poor conditions	
Fair conditions	
No data	

Table 6: Fair, average and poor seeing conditions from April 1987-April 2000

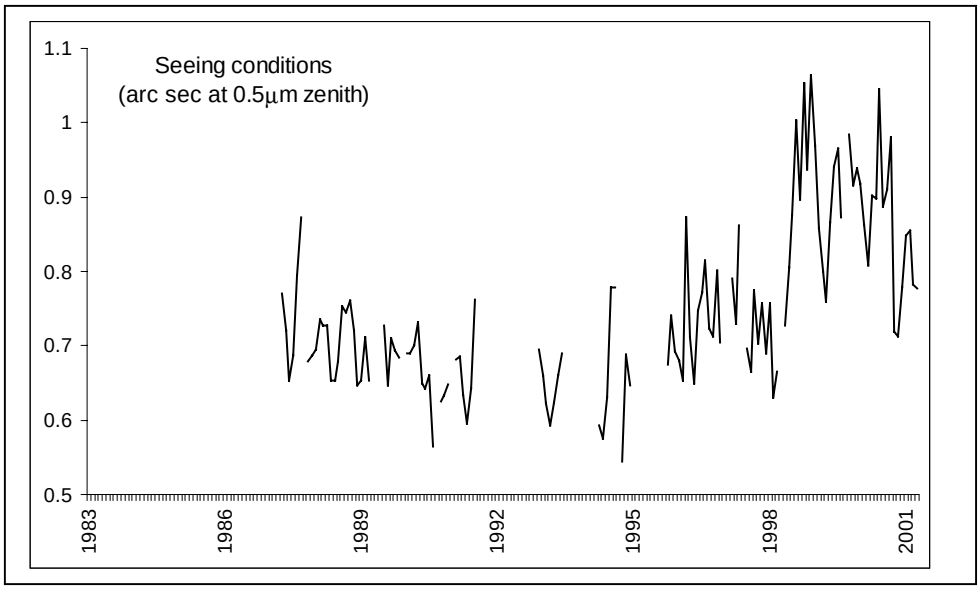

Figure 7: Monthly-mean time series of seeing at Paranal

In Figure 7, it is seen that there are several “blocs” of data. The first occurs between April 1987 and September of the same year, with four values above the mean and two below. The lowest range of the series occurs in October 1990 (0.565) and a set of moderate values around 0.763 (July 1991) et de 0.779 in July and August 1994, with a minimum in this bloc of 0.544 in October 1994. A further data bloc exhibits values from 0.65 (May 1996) to 0.815 (August 1996), and the lowest value recorded in February 1998 (0.631). From this date onwards, the value of the seeing parameter steadily increased (reduced quality of astronomical observations) to 0.875 in July 1998. ESO considers that visibility deteriorated significantly from August 1998, where the seeing parameter at Paranal exceeded 1 on a number of occasions, namely 1.003 (August 1998), 1.053 (October 1998), 1.064 (December 1998) and 1.045 (June 2000). The lowest values in this period are still representative of “poor” seeing conditions, such as 0.759 (April 1999) and 0.808 (March 2000). A marginal amelioration has been recorded in the latter part of the year 2000, with 0.712 in November 2000; however, values have risen once again to 0.855 in February 2001.

4.7. Reconstructing the observational record at Paranal

Because the meteorological observations at Paranal span a relatively short time frame (1985-present), and because there are a number of gaps even in this short record, it is necessary to find an alternate method to close these gaps and to extend the Paranal record back in time. The main reason for undertaking this procedure is to allow an assessment of whether other periods in the past exhibit similar characteristics to those which have recently been causing problems for astronomical observations for the ESO VLT (Very Large Telescope).

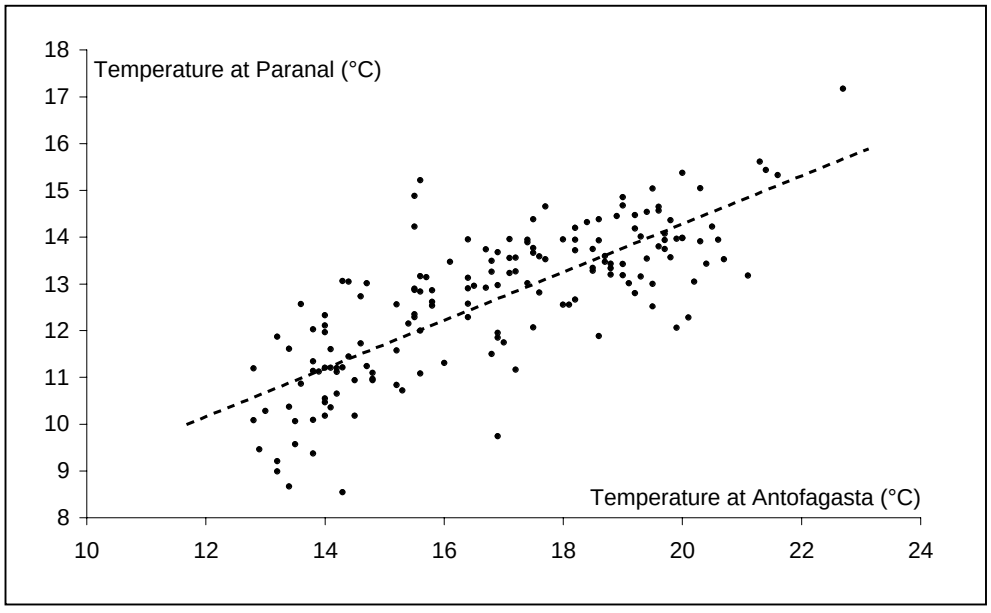

Figure 8: Correlation between monthly-mean surface (2 m) temperature records at Antofagasta and Paranal

Analysis of the Paranal and Antofagasta records show that there is a synchronous behavior of the two time series, as seen in Figure 8; the correlation between the two sets of data is 0.77. This implies that climatic conditions at Paranal are also highly sensitive to ENSO conditions in the Pacific, despite the high elevation of the Paranal site and the fact that it is located well above the maritime boundary layer within which Antofagasta is located. It is thus legitimate and scientifically sound to use the Antofagasta temperature record as a "proxy" to reconstruct climate series at Paranal. The smoothed curves for the two time series are given in Figure 9; for any reconstruction by analogy with Antofagasta, the Paranal data of course needs to be corrected for altitude.

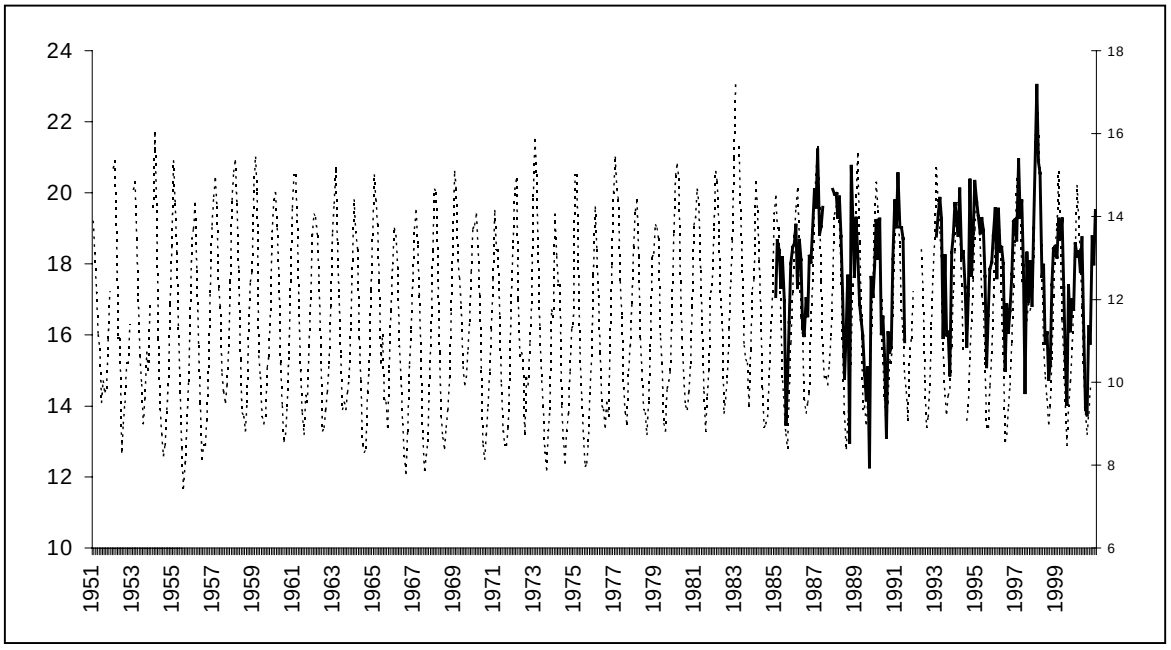

Figure 9: Time series of monthly-mean temperature at Antofagasta (dotted line: 1951-present) and at Paranal (solid line: 1985-present, with certain gaps in the series)

The long-term trend in temperature at Antofagasta is a very low 0.11°C per century, based on the 1951-2000 time series given in Figure 9; statistically-speaking, the trend is not significant. The rate of warming at Antofagasta is almost one order of magnitude lower than the global-average warming observed since 1900 (Jones et al., 1999). At Paranal itself, over the short period of observational record, the warming trend is even less significant (0.02°C per century, based on the 15 years of data). Direct regional warming can therefore be ruled out as a significant driving factor for changes in astronomical observation conditions.

By looking at the two series in Figure 9, it can be surmised that other periods of lower than average seeing conditions have occurred in the past; those that are not included in the Paranal record may be captured by analogy with the Antofagasta record. An obvious example is the 1982-1983 El Niño

event and the subsequent cold phase of ENSO, whose “signature” in Figure 9 closely resembles that of the latest event in 1997 and subsequent years. This topic will be revisited in a later section of this report.

5. Possible causal mechanisms for differences in seeing conditions

The previous section has shown unambiguously that long-term climatic change is not a candidate to explain the changes in seeing that have been responsible for less optimal conditions since 1998, but rather that the El Niño/Southern Oscillation (ENSO) mechanisms represent the dominant mode of climate variability in the region. Furthermore, the poorer seeing conditions are associated with the cold phase of ENSO, which in the last ENSO episode developed in mid-1998 and resulted in one of the strongest and most persistent La Niña events on record. It is thus of interest to assess the fundamental changes that are occurring in the general vicinity of the south-eastern Pacific and central Latin America. This can help identify the processes responsible for changes in astronomical seeing conditions.

In order to achieve this objective, two particular periods have been selected, namely those with the best seeing conditions of the Paranal observational period for typical spring (October) and autumn (May) months. In the present study, the worst seeing conditions of the record are observed in October 1998 and in May 2000; the most optimal seeing conditions are recorded in May 1994 and October 1994. The discussion will thus focus on the differences in the monthly means of large-scale and regional scale atmospheric patterns between these extremes to determine whether there is a systematic bias in weather conditions between periods when La Niña conditions prevail, and other climatic situations. Four climate-relevant variables are considered in this section, namely:

- geopotential height, i.e., the height of a particular pressure surface, whose level is determined by the integrated temperature in the column of air between the ground and the selected pressure level
- wind velocity
- relative humidity
- cloud-induced net long-wave radiation. This latter parameter allows an indirect measure of the presence of clouds and moisture through the relative influence these phenomena exert on the reduction of outgoing terrestrial radiation.

5.1 Geopotential height (m)

A typical La Niña is accompanied by a tongue of colder-than-average SSTs in the tropical southern Pacific. A zone of relatively high pressure builds up to the south of the cold tongue, exemplified by

a thickening of the layer and a upward shift of the 700 hPa pressure surface. The 700 hPa geopotential height is the standard pressure level closest to the altitude of Paranal (2,635 m above sea level). This middle atmosphere pressure system is located south of about 20-25° S, off the western coast of Chile (see Figure 10a for May 2000 and 10b for October 1998). The height of the 700 hPa level is on average 3140 m, and thus the height anomaly at the center of the high-pressure system is about 40 m, which represents a strong departure from mean geopotential height (Figure 11a for May 2000 and 11b for October 1998).

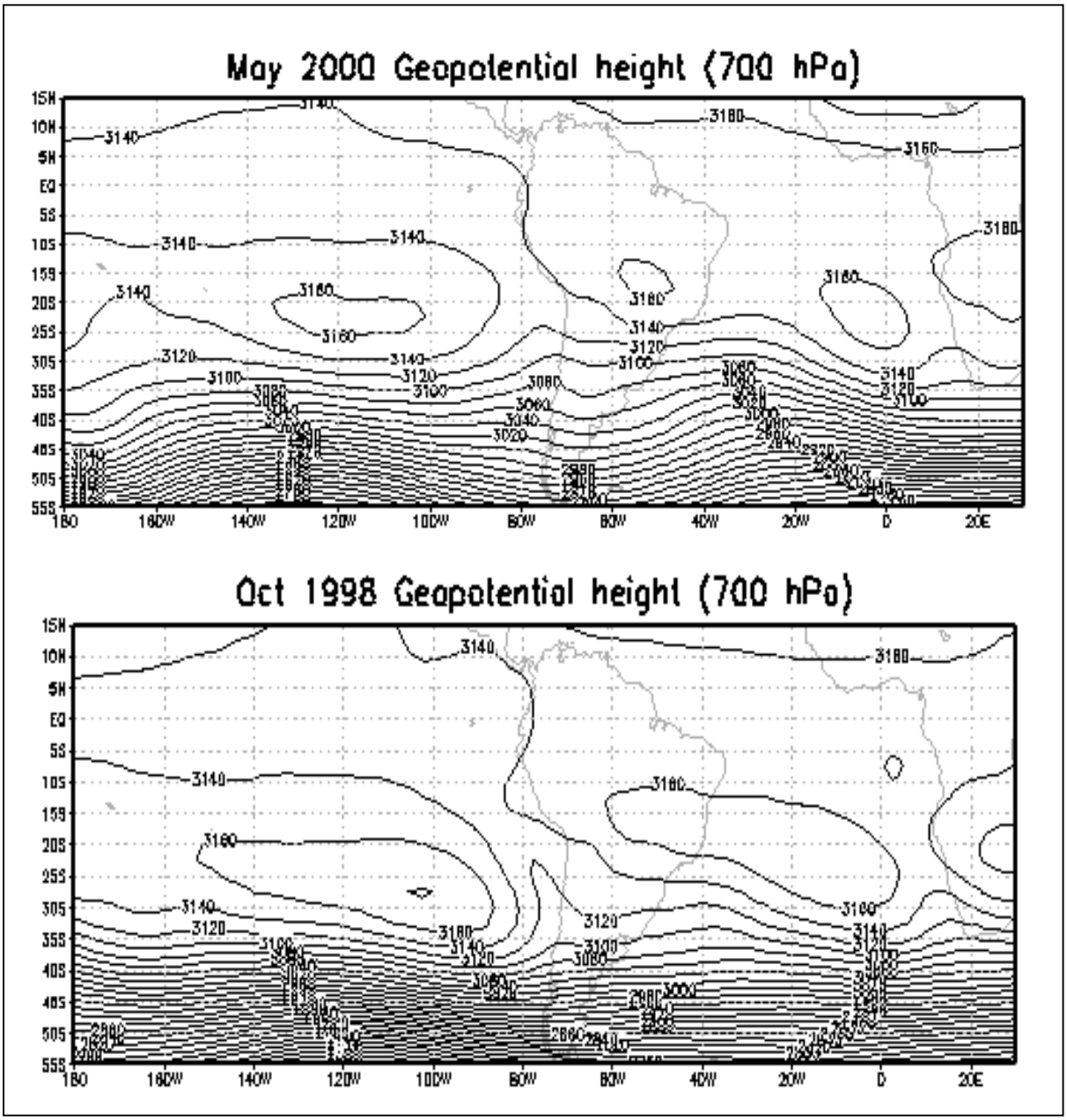

Figure 10: 700 hPa geopotential field for South America and the eastern Pacific for a) May 2000 and b) October 1998

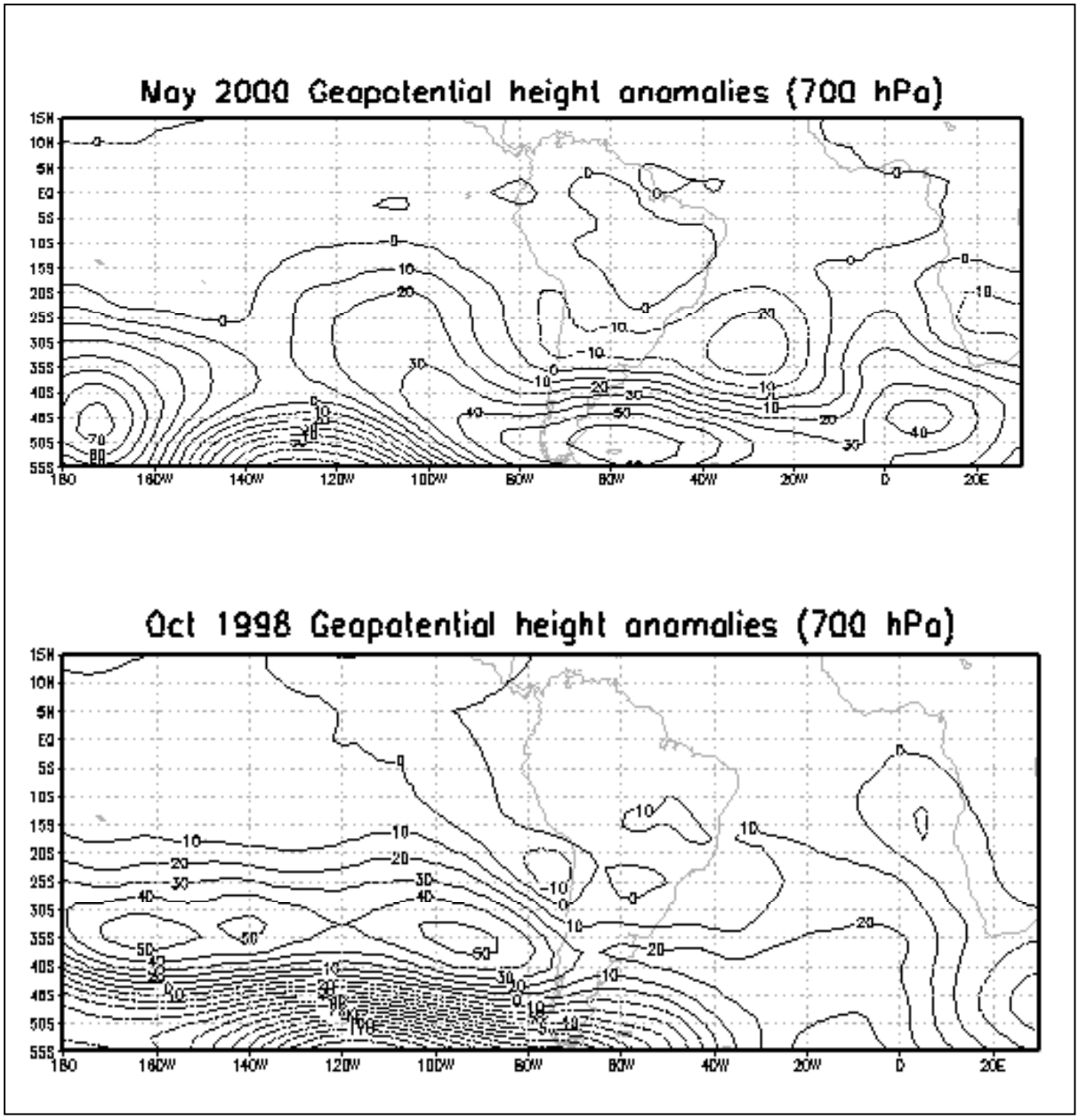

Figure 11: As Figure 10, except for geopotential height anomalies

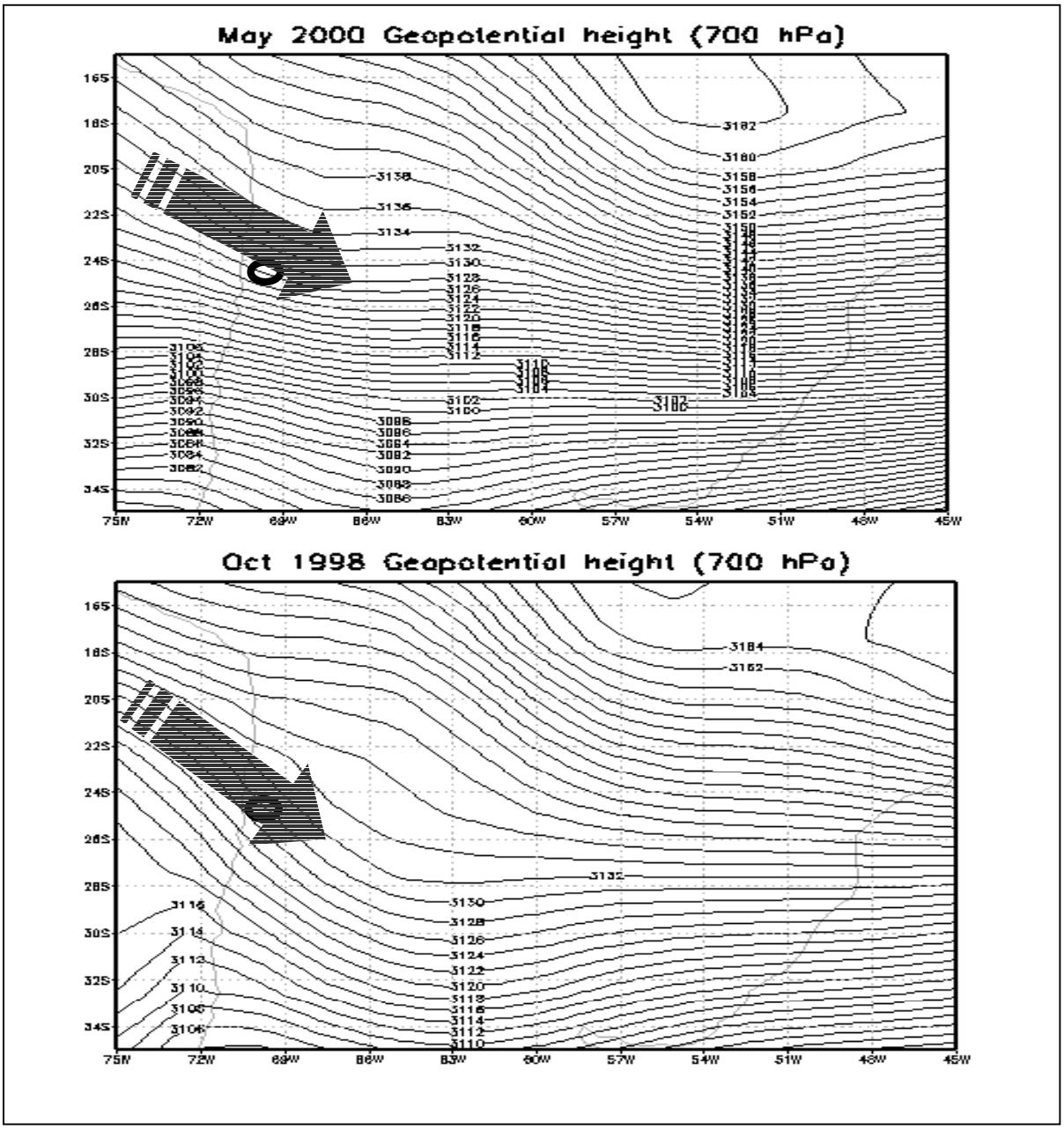

Figure 12: 700 hPa geopotential field for the central portion of Latin America, providing details on the height distribution over the Paranal area for a) May 2000 and b) October 1998. The circle is centered on the ESO Paranal site.

Over Bolivia and southern Brazil, a secondary cell of high pressure is also observed, more extended in October 1998 than in May 2000, which may be related to the particular intensity of La Niña recorded in October 1998. A trough of lower geopotential values is located between the two large-scale pressure patterns, whose negative anomalies can exceed 10 hPa. This middle-troposphere trough is oriented SE-NW, stretching from the Santiago area well into the tropical Pacific far offshore from Ecuador and Peru. At Paranal itself, the geopotential height anomalies during the two selected La Niña months reach –6 to –10 m (Figure 11). The general flow pattern at the 700 hPa level, unperturbed by orography, is parallel to the isopotential lines, with lower heights located to the right of the flow direction.

Hence, synoptic flow enters the Paranal area from a WNW-NW direction, bringing with it characteristics of air originating close to the Equatorial zone above the Pacific. The close-up maps of the geopotential for the central part of Latin America given in Figures 12a for May 2000 and 12b for October 1998 emphasize this general tendency. Further south, the flow is essentially of a westerly nature, typical of the middle latitude circulations.

During good seeing conditions in 1994, the synoptic situation is considerably different from that just described, as shown in Figure 13a and 13b for the two selected months, respectively. The high-pressure system over the eastern Pacific is either non-existent or much weaker and located much further west over the Pacific than during El Niño, whereas the high-pressure system over Brazil is shifted further to the east. In May 1994 (Figure 13a), for example, this high-pressure cell is even located offshore of Brazil in the southern Atlantic. The corresponding geopotential anomaly charts illustrated in Figues 14a and 14b exhibit little anomalies in the Chilean region and even a slight positive anomaly in May. The direction of the synoptic flows is essentially from the W, with a slightly more WNW component in the case of May 1994. However, the source region from which these middle-tropospheric winds blow is located far to the south of the source region during the La Niña phase, so that the atmospheric characteristics advected along the 700 hPa surfaces are significantly different from those occurring during La Niña. Figures 15a and 15b for May 1994 and October 1994, respectively, show the close-up details of the 700 hPa geopotential height for central Latin America. In October 1994, a slight upper-air ridge located to the NW essentially decouples air flows reaching Paranal from the tropical Pacific, which is the exact opposite of what occurs during the La Niña phases of ENSO.

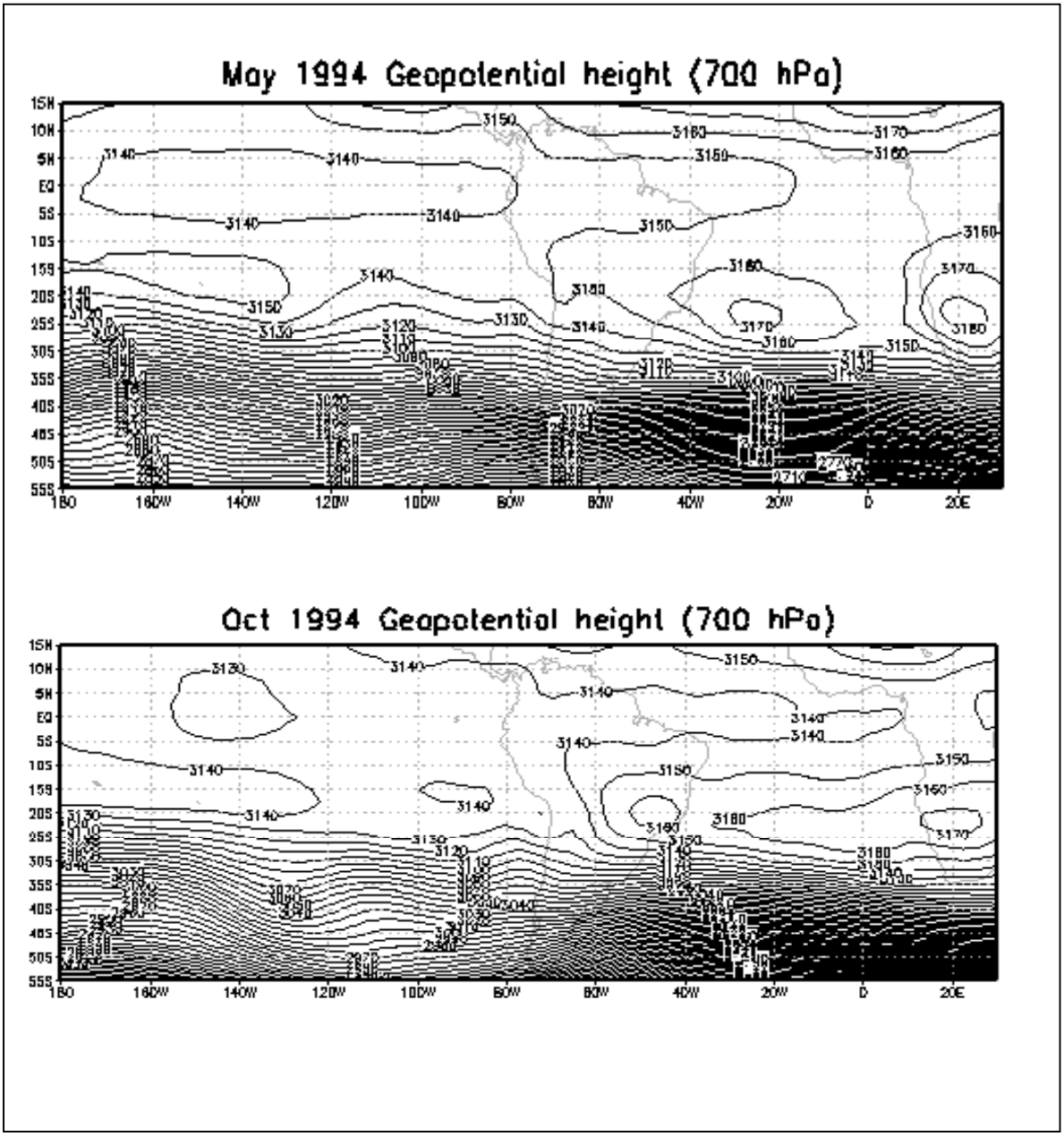

Figure 13: 700 hPa geopotential field for South America and the eastern Pacific for a) May 1994 and b) October 1994

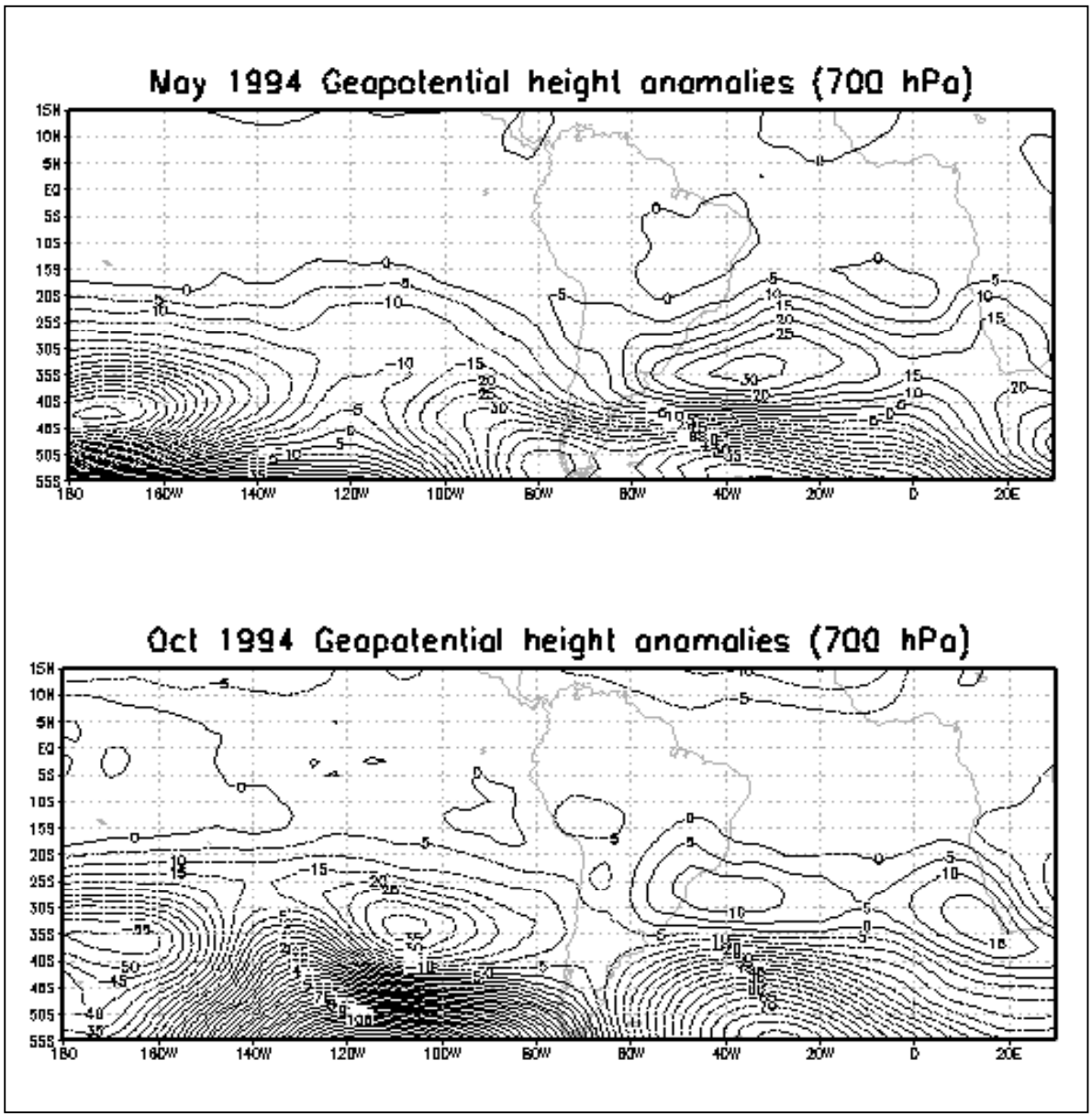

Figure 14: As Figure 13, except for geopotential height anomalies

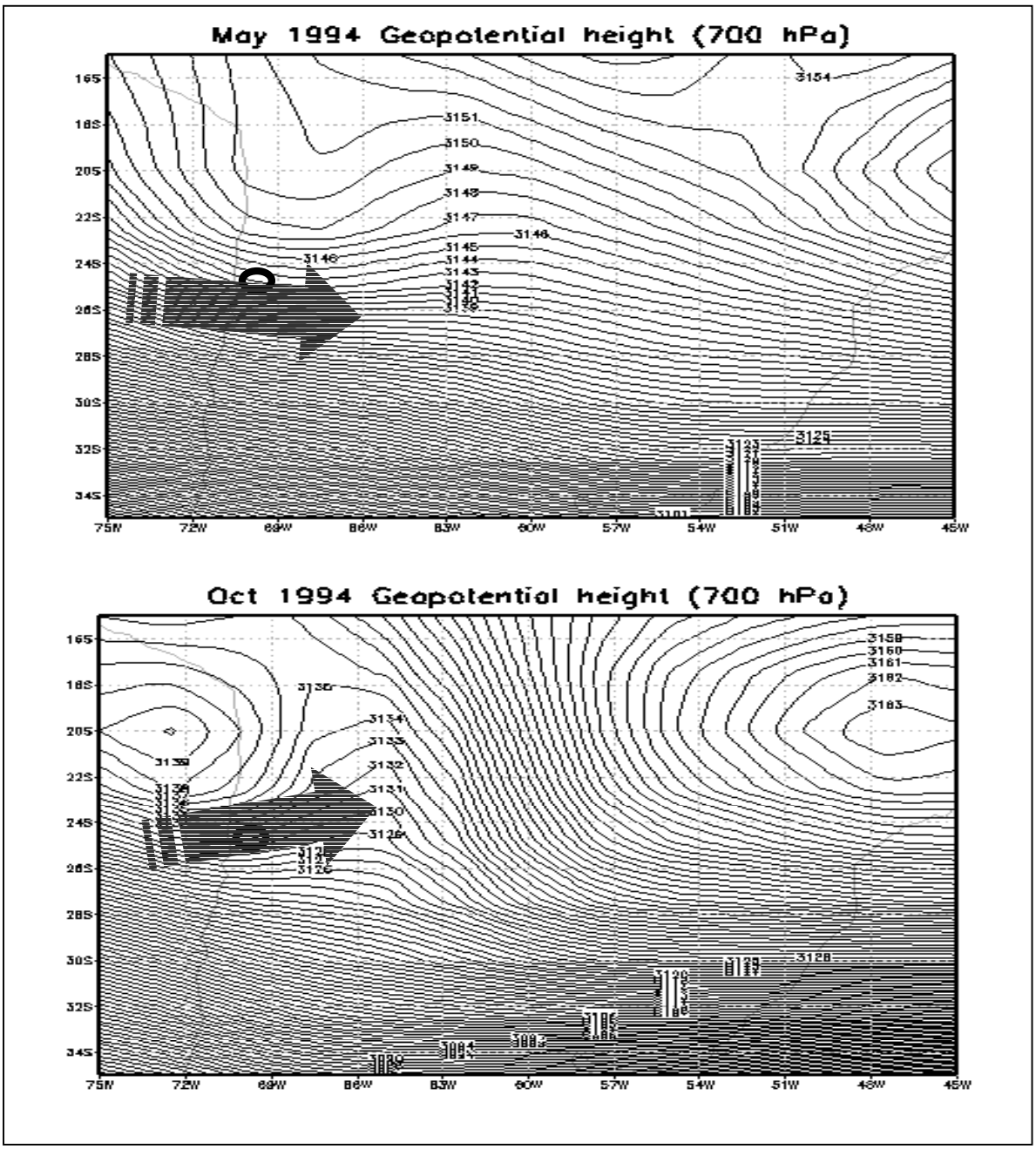

Figure 15: 700 hPa geopotential field for the central portion of Latin America, providing details on the height distribution over the Paranal area for a) May 1994 and b) October 1994. The circle is centered on the ESO Paranal site.

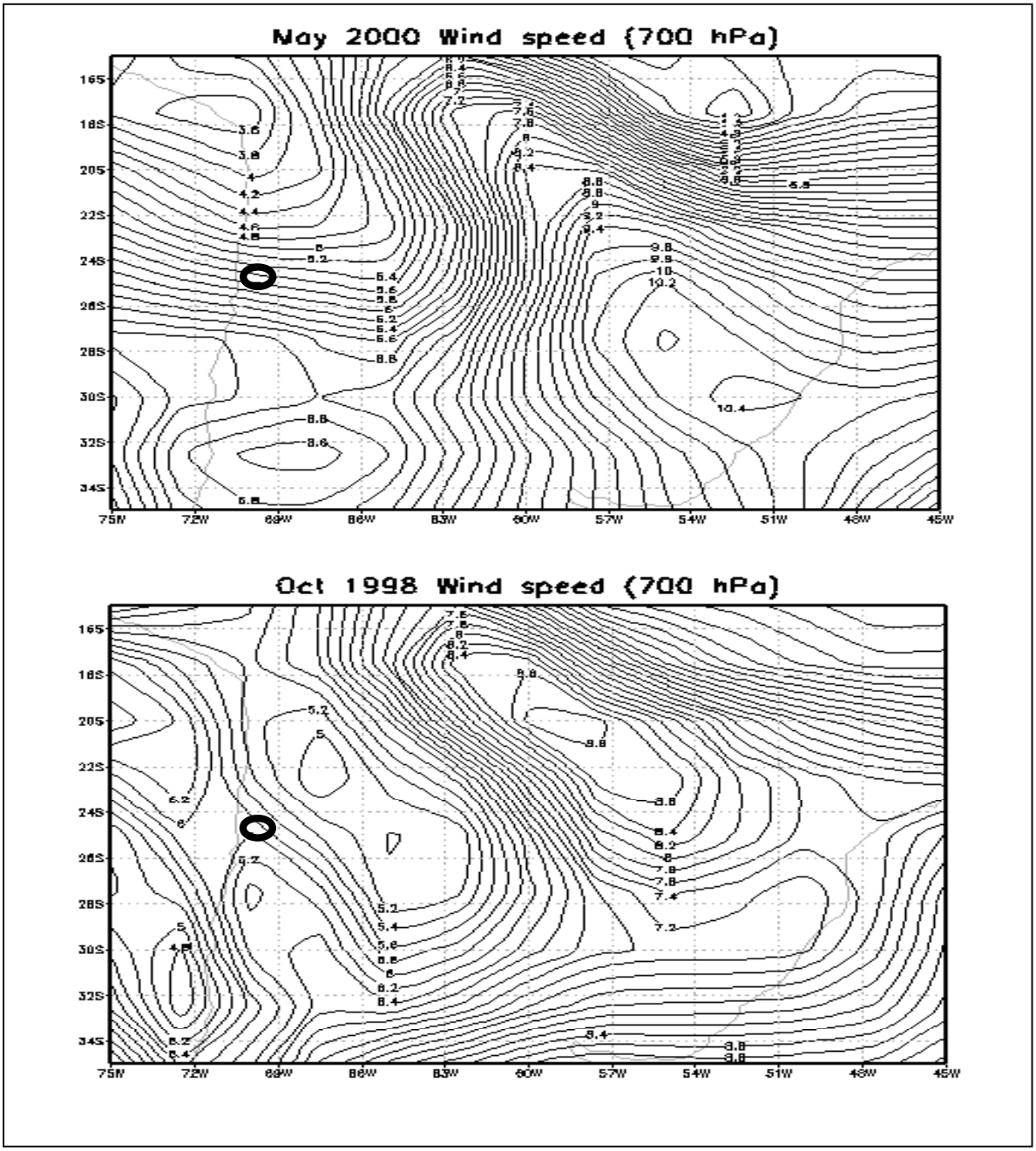

Figure 16: Wind velocity field for the central portion of Latin America, providing details on the velocity distribution over the Paranal area for a) May 2000 and b) October 1998. The circle is centered on the ESO Paranal site.

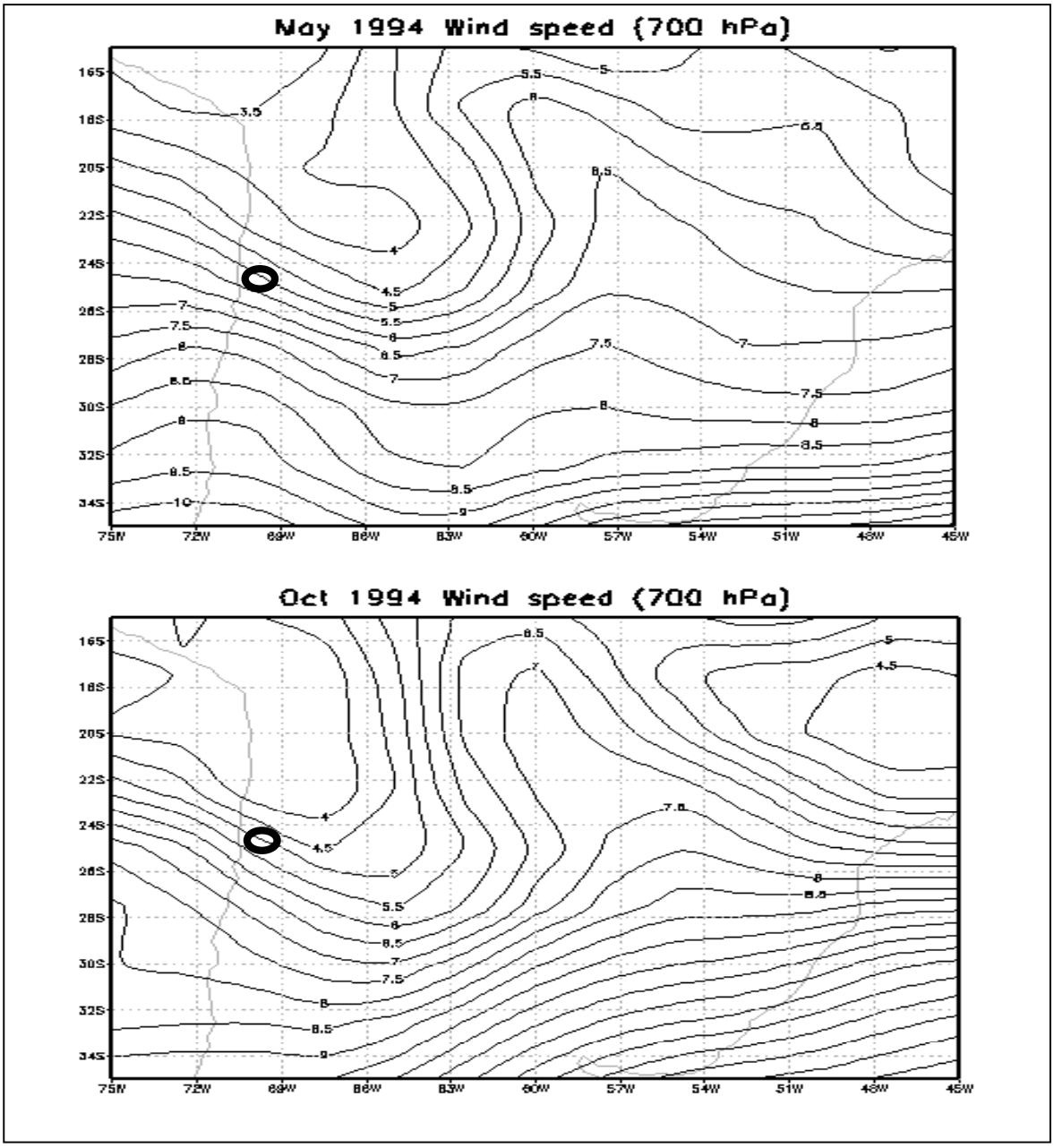

Figure 17: Wind velocity field for the central portion of Latin America, providing details on the velocity distribution over the Paranal area for a) May 1994 and b) October 1994*. The circle is centered on the ESO Paranal site.*

5.2 Wind speed (m/s)

Figure 16a and 16b show the mean wind-speeds recorded at 700 hPa over the central portion of Latin America during periods of lower-than average seeing, i.e., for May 2000 and October 1998, respectively. Because of the relatively tight geopotential gradients described previously, the wind velocity pattern indicates fairly rapid flow over the Paranal region, exceeding 5 m/s. For the optimal seeing conditions in May and October 1994, Figures 17a and 17b show marginally lower wind velocities, ranging from 4.3 to 4.8 m/s at Paranal. Wind velocity alone cannot explain the reduction

in seeing capacity at Paranal, even if it may be argued that turbulent fluctuations may be sufficiently enhanced by this velocity difference (as turbulence is essentially proportional to the square of wind speed). A slight increase in mechanical turbulence may therefore be expected, thereby generating disturbances in the atmospheric stratification, possibly resulting in more shimmering. This is because the NW orientation of the flow under La Niña conditions allows the air to be in contact over a longer distance (i.e., for a longer time) with the roughness elements of the continental surface than when the flow is oriented in a westerly direction and transits rapidly from the ocean to the Paranal area.

5.3 Relative humidity (%)

On average throughout the year, relative humidity is about 15%, but has an annual cycle in which maximum values are recorded in December and January, at the height of the southern hemisphere summer when moisture convergence raises the humidity levels beyond 30%. May is often slightly moister than October, records for the latter month sometimes showing relative humidity values less than 5% on a monthly-average basis.

During periods of lower than average seeing conditions, relative humidity increases sharply in the northern part of the Chilean Andes, as a result of the advection of moist air originating in the tropical Pacific. This influx of air masses from the tropical zone is a consequence of the flow directed parallel to the isolines of geopotential height, as discussed previously. Figure 18 shows the concentration of relatively moist air at the 700 hPa level along the Peruvian Andes, and the curvature of this moist zone southwards into northern Chile. More detailed mesoscale analyses at the 300 hPa level suggest that air entrained from the NW may originate from the Bolivian region, cross over the Pacific offshore from Peru, and then flow in a south-easterly direction towards northern Chile (Erasmus, 1998). These finer-scale details cannot be observed in the 700 hPa synoptic-scale fields, however.

While on average, the relative humidity at Paranal is around 20% or less, making it one of the driest regions of the planet, La Niña and associated atmospheric circulations serve to increase the values of relative humidity to around 40% in both the May 2000 and the October 1998 cases. While this may still be considered to be very dry compared to mid-latitude Europe, for example, this doubling of relative humidity nevertheless implies a substantial increase of water vapor in the Andean atmosphere. Such an increase in moisture has the potential for thin cloud formation at higher elevations in the troposphere, as will be shown later, with a potential for poorer conditions for certain types of astronomical observations.

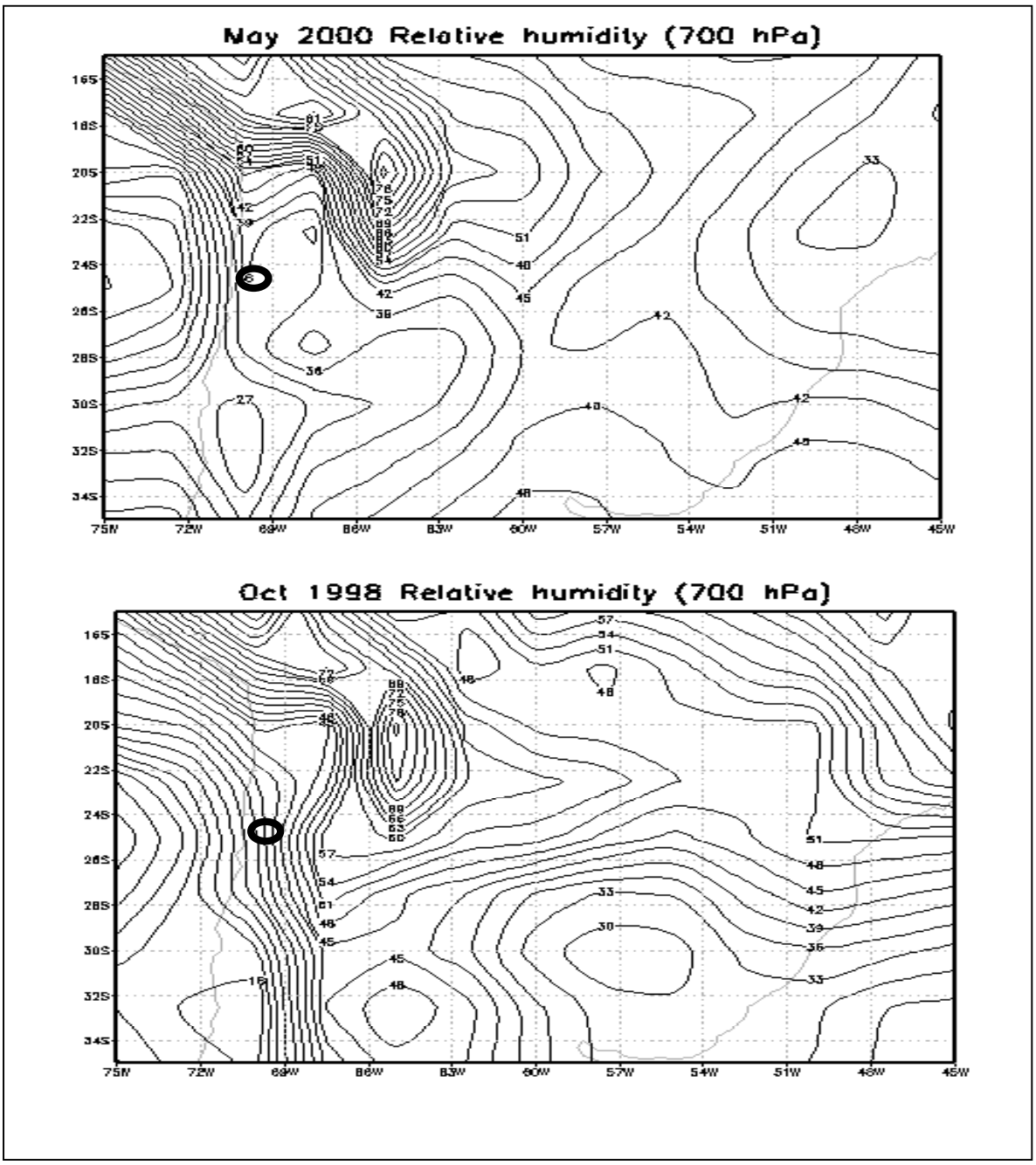

Figure 18: Relative humidity field at 700 hPa for the central portion of Latin America, providing details on the moisture distribution over the Paranal area for a) May 2000 and b) October 1998. The circle is centered on the ESO Paranal site.

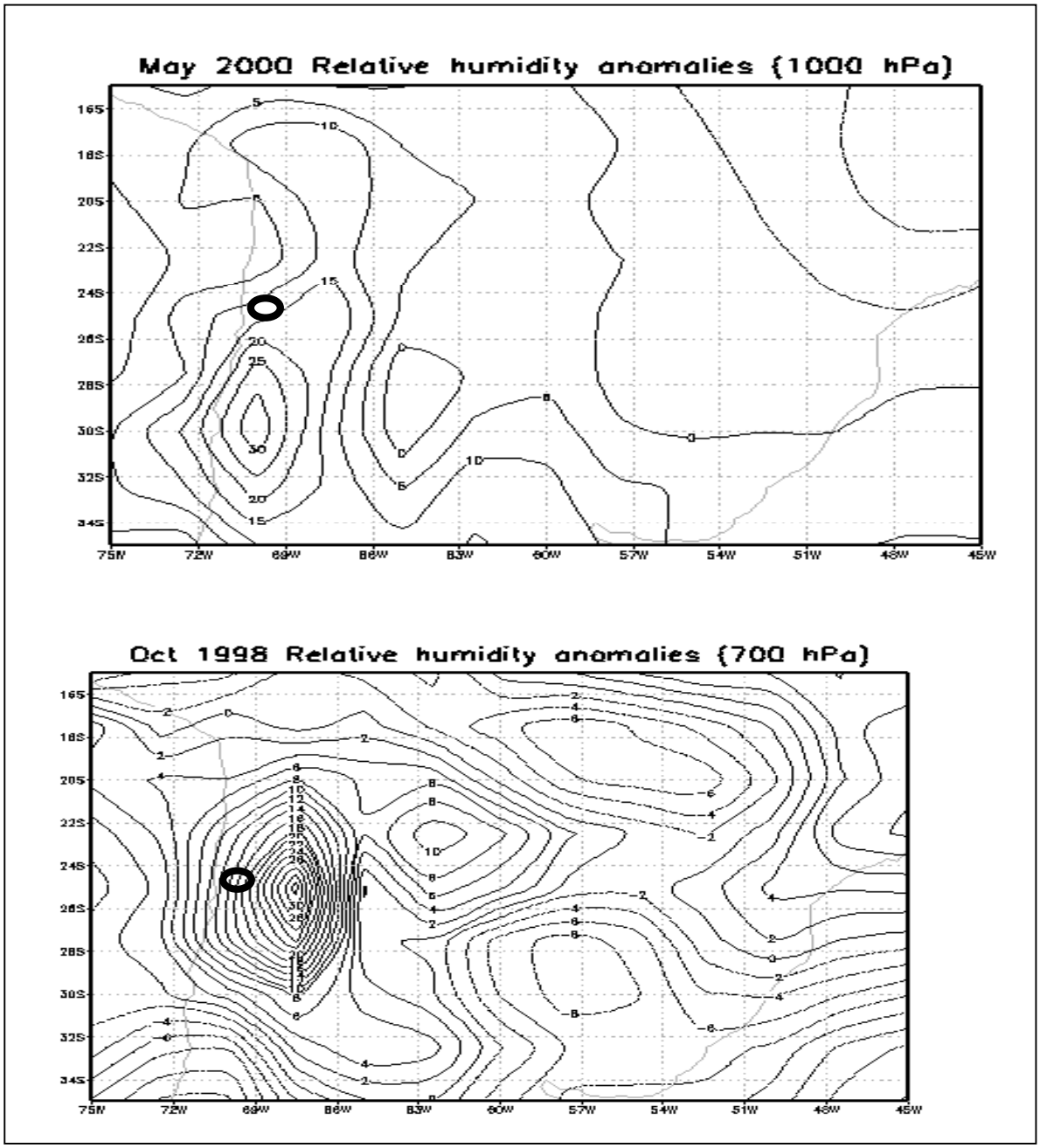

Figure 19: 700 hPa relative humidity anomaly field for the central portion of Latin America, providing details on the moisture distribution over the Paranal area for a) May 2000 and b) October 1998. The circle is centered on the ESO Paranal site.

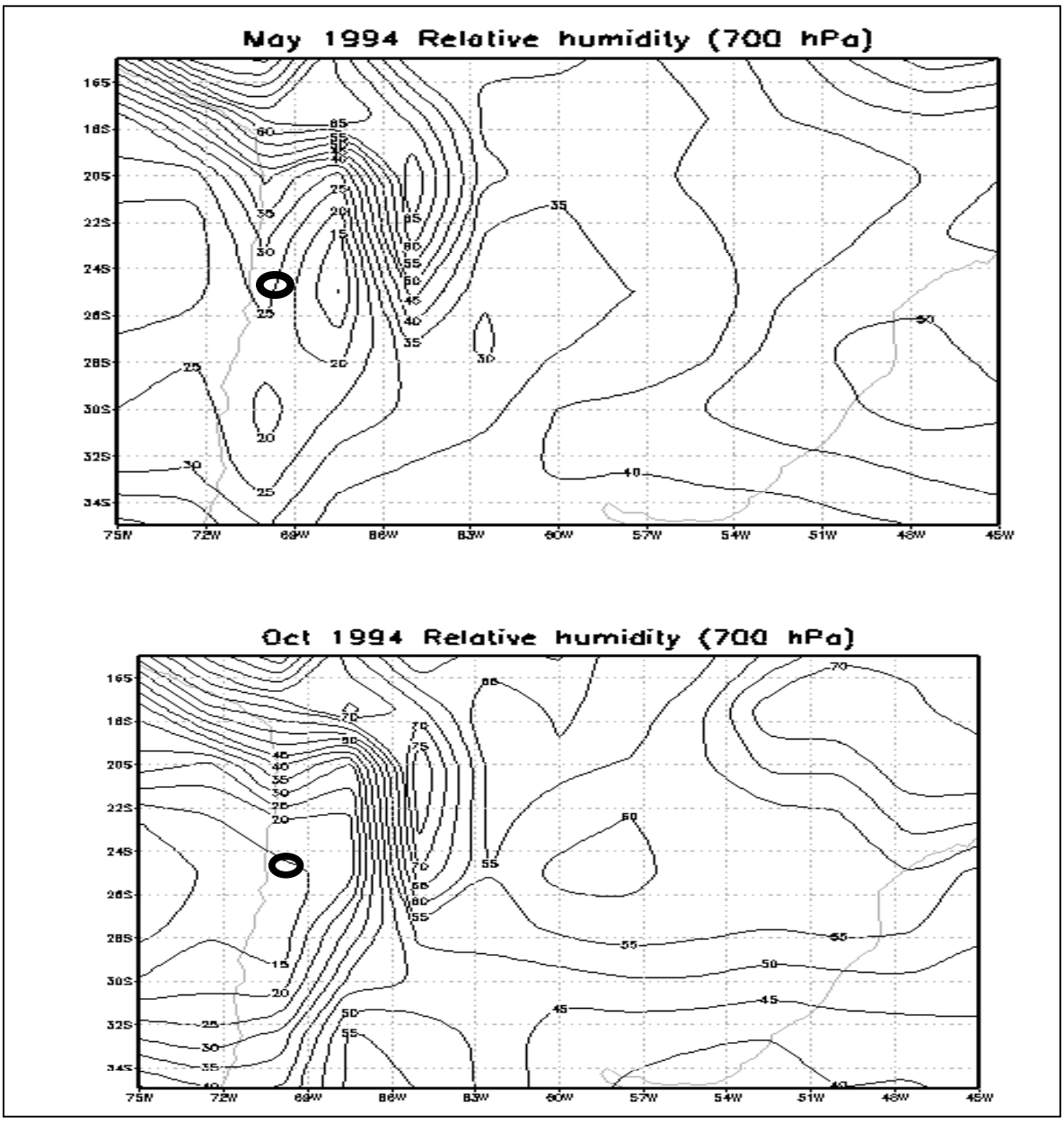

Figure 20: 700 hPa relative humidity field for the central portion of Latin America, providing details on the moisture distribution over the Paranal area for a) May 1994 and b) October 1994. The circle is centered on the ESO Paranal site.

The corresponding anomaly maps for the Pacific-Latin America region (Figure 19) clearly shows that it is particularly the northern part of the Chilean Andes that experiences the sharpest positive relative humidity anomalies anywhere over the South American continent. Particularly in Figure 19b (October 1998), the source region of the moisture at 700 hPa, according to the synoptic analyses may be located offshore from Peru and Ecuador, in a region confined between 80° and 100°W and between 5° and 15°S. However, as shown by Erasmus (1998) and discussed previously, the

moisture may actually originate in Bolivia and may follow a circuitous route over Peru, over the ocean, and southwards to Chile. Whatever the source, however, moisture convergence tends to increase relative humidity in much of the Andean chain; some of this high moisture spills over into the coastal ranges of northern Chile and thereby affects Paranal. The positive anomaly zone stretches further to the SE into Argentina, well beyond the boundaries of the Andes.

Figure 19 serves to highlight the relative humidity anomalies over the region of interest. The positive anomalies at Paranal are clearly apparent both in May 2000 (Figure 19a) and October 1998 (Figure 19b). The core of the anomaly distribution is located some 200 km to the SE of the ESO VLT. If a good correlation exists between seeing and relative humidity, it may well be because the conditions responsible for increases in relative humidity are those that are also responsible for perturbations to the atmospheric temperature stratification. For periods where the seeing conditions at Paranal are better than average, the relative humidity values are 5-7% lower than the long-term average over the region at the 700 hPa level for that particular location in May 1994 (Figure 20a) and October 1994 (Figure 20b). These very low values, both in absolute terms and in terms of the anomalies of relative humidity, reduce the risk of cloud cover and tend to offer optimal seeing conditions. The relation between the relative humidity and seeing conditions is illustrated in Figure 21; the correlation between the data sets is 0.75, which implies that 55% of the variance in seeing conditions are related to fluctuations in relative humidity.

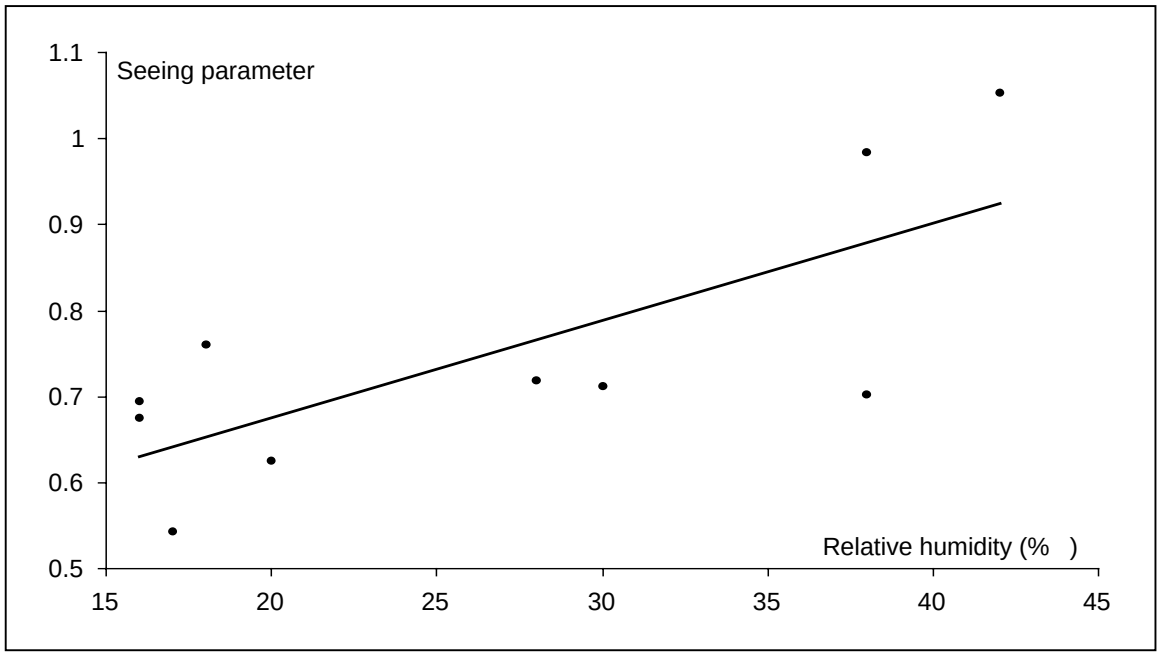

Figure 21: Relation between relative humidity and seeing for different climatic situations at Paranal during the months of October 1988, 1989, 1990, and 1994-2000.

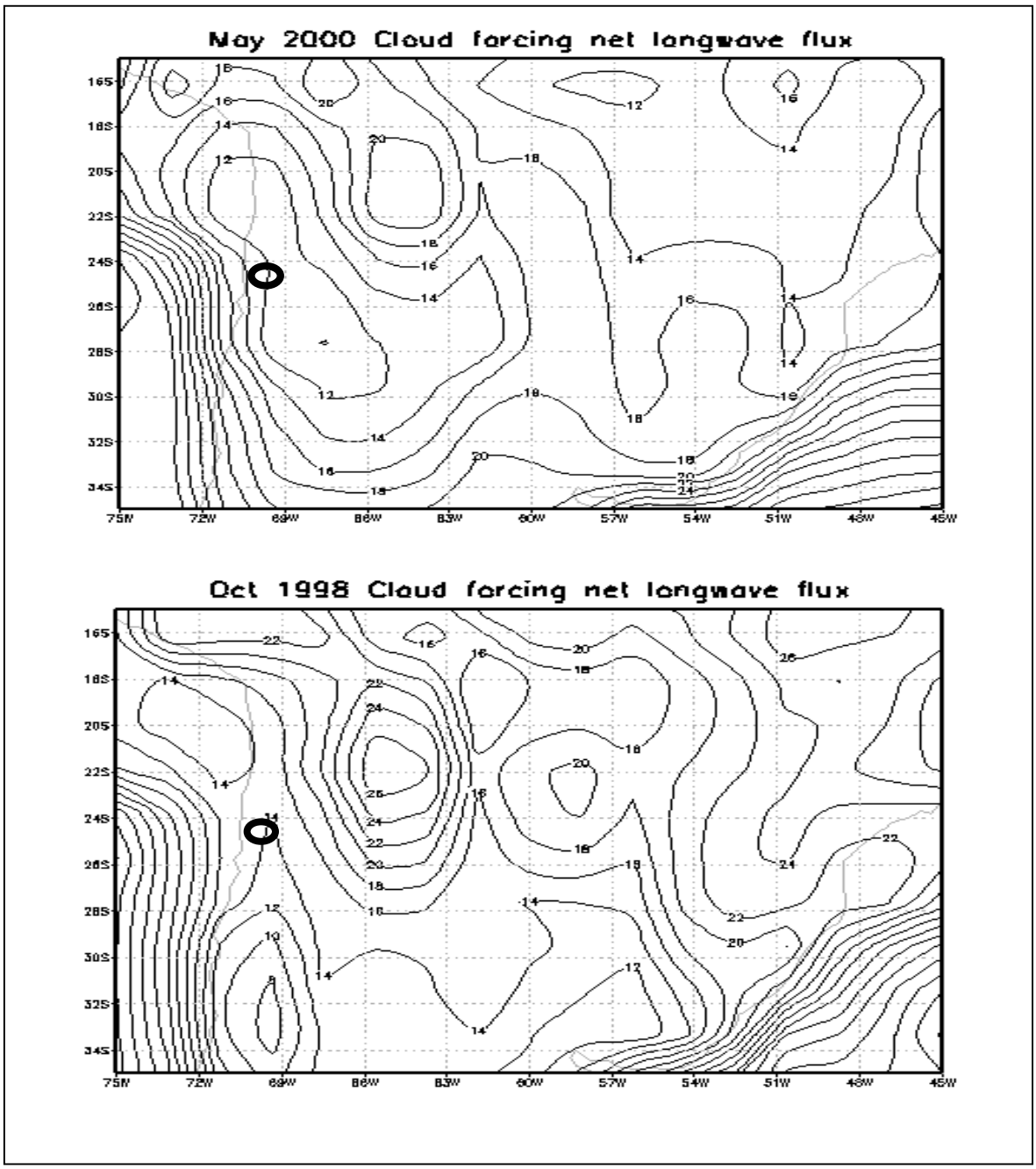

Figure 22: Cloud forcing net longwave fluxes for the central portion of Latin America, providing details on the longwave flux distribution over the Paranal area for a) May 2000 and b) October 1998. The circle is centered on the ESO Paranal site.

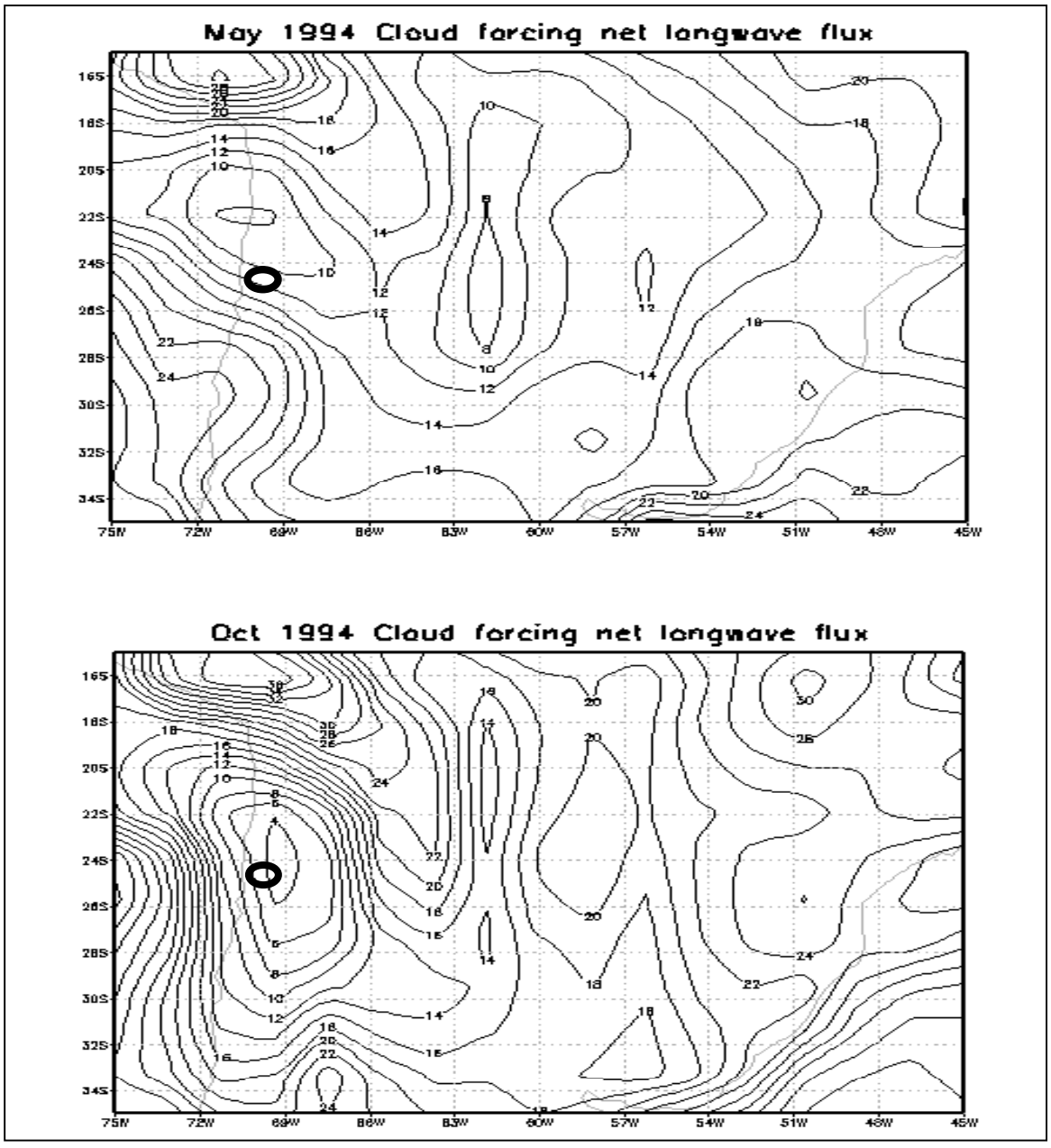

Figure 23: Cloud forcing net longwave fluxes for the central portion of Latin America, providing details on the longwave flux distribution over the Paranal area for a) May 1994 and b) October 1994. The circle is centered on the ESO Paranal site.

5.4 Cloud forcing net longwave flux (CFNLF, W/m^2)

The cloud forcing net longwave flux (CFNLF) allows an indirect assessment of the presence of clouds by integrating the changes in longwave terrestrial radiation between the ground surface and the upper atmosphere. Hence, an increase in the longwave flux in any given region signals the

presence of some form of cloud liquid water or ice, which reduces the outgoing longwave radiation by increasing the opacity of the atmosphere to infrared wavelengths. It is also a parameter which, in terms of perturbations to seeing, is more useful than water vapor, in the sense that it is a measure of the possible presence of clouds when direct cloud observations are not possible. The possible presence of clouds is a factor which the analyses of relative humidity alone do not allow. While the CLNWF does not tell us anything about the type of cloud that may be present, it can be assumed that any small increase in its value may be associated with very thin high-altitude clouds, such as cirrus. These clouds are often undetected by the naked eye, but have the potential of perturbing precise astronomical observations by the VLT.

Figure 22 shows the distribution of CFNLF over the central Latin America domain. While the core of elevated values of CFNLF is located to the NE of the ESO site, the values at Paranal range from 12-15 W/m^2, up from less than 9 W/m^2 in May 1994 (optimal seeing conditions for May) and 3 W/m^2 in October 1994 (optimal seeing conditions for October), as illustrated in Figure 23. The La Niña type of synoptic situation brings with it sufficient moisture to allow the formation of thin clouds above the ESO astronomical observational site, with the consequent reduction of the seeing conditions which this entails. Indeed, Figure 24 provides an example of the relation between CFNLF and seeing at Paranal for the range of higher and lower than average seeing conditions considered here. Close to 55% of the variance of seeing conditions can be explained by CFNLF and, hence, by the possible presence of thin clouds. The correlation coefficient between CFNLF and the seeing parameter is 0.74, which is highly significant and is certainly related to the same causal mechanisms that are responsible for poor seeing conditions.

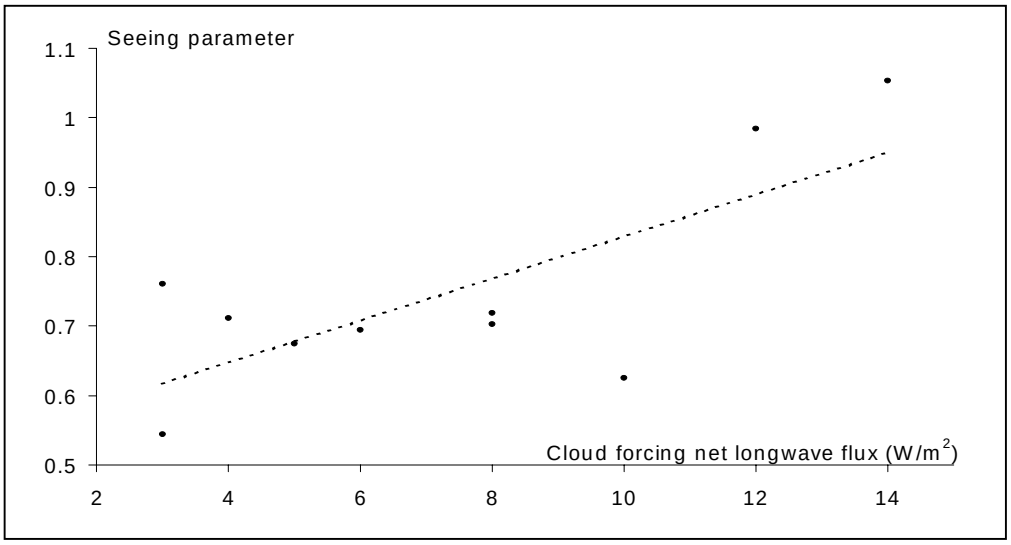

Figure 24: Relation between cloud forcing net longwave fluxes and seeing for different climatic situations during the months of October 1988, 1989, 1990, and 1994-2000.

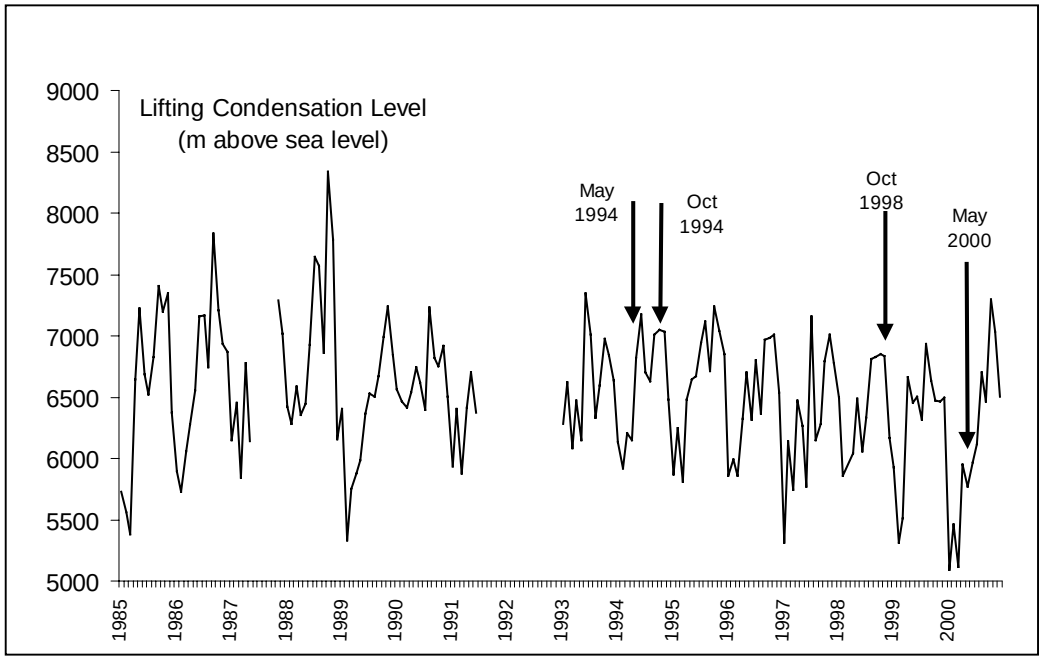

Figure 25: Computed lifting condensation level for Paranal. Arrows indicate the periods of favorable and less favorable seeing

Figure 25 provides a time-series of the lifting condensation level at Paranal, which is the theoretical level at which moisture would condense if lifted sufficiently high into the atmosphere. This is computed on the basis of the known values of relative humidity (U), temperature (T) and pressure (p), and assuming a dry adiabatic lapse rate ($\partial t/\partial z$ = -9.8°C/km) in this very dry atmosphere. Once the dew-point temperature (T_d) is computed from U, T, and p, the difference between T_d and T divided by the lapse-rate $\partial t/\partial z$ provides an estimate of the height of the layer where condensation is likely to occur. The range of possible condensation levels is seen to vary considerably, from just over 5000 m above sea level to well above 8000 m. May and October 1994 exhibit potential condensation levels at around 7000 m. For the poor seeing conditions, the condensation level for October 1998 is 6840 m, and for May 2000 is 5940 m. At these elevations, any moisture which does actually condense will enter into the ice phase, because of the extremely cold conditions which prevail in the middle troposphere. While the altitude of the lifting condensation level is essentially decorrelated from the seeing parameter, the CFNLF clearly is not. Thus, the CFNLF indicates whether some measure of condensation has taken place, and the lifting condensation level at which height above sea level the phase transition of water occurs. The height of this level is such that condensate will always be in the ice phase, i.e., most frequently in the form of thin cirrus, which are capable of interfering with certain types of astronomical observations.

5.5 Consistency with other periods in which seeing conditions are lower than average

In order to confirm the systematic nature of the conclusions discussed above, a number of other situations with above or below average seeing conditions have been selected. The data are provided in tabular form in Table 7 for the months of May and October in which seeing conditions are either above or below average. The seeing parameter is on average 0.75 for the period of the observational record at Paranal, and one standard deviation (σ) is 0.113. Thus, any departure by at least 2 standard deviations or more can be considered to represent particularly good or particularly poor conditions for astronomical observations. On this basis, representative examples that have been chosen for good seeing conditions include May 1991 and October 1999 for less optimal conditions. In the former case, the equatorial Pacific was in a normal phase preceding the 1992 El Niño outbreak, while the latter case is representative of the strong and persistent La Niña phase which succeeded the strongest 20th Century El Niño event of late 1997. This La Niña event was observable from the late Spring of 1998 and persisted until late 2000, which is an unprecedented duration for the cold ENSO phase.

	Months of May									
	1989	1991	1994					**1998**	**1999**	**2000**
Seeing	.638	.596	.575					**.728**	**.866**	**.896**
Geopotential	3145	3148	3145					**3140**	**3138**	**3130**
Wind speed	5.0	4.6	4.8					**4.1**	**4.3**	**5.2**
Rel humidity			22							**37**
Cloud LW	7	8	9					**8**	**8**	**11**
	Months of October									
	1989	1990	1994	1995	**1988**	**1996**	**1997**	**1998**	**1999**	**2000**
Seeing	.694	.625	.544	.675	**.761**	**.712**	**.703**	**1.053**	**0.984**	**0.719**
Geopotential	3140	3139	3132	3130	**3129**	**3129**	**3120**	**3132**	**3128**	**3126**
Wind speed	3.5	5.0	4.4	3.9	**4.2**	**4.2**	**6.5**	**5.5**	**5.4**	**3.5**
Rel humidity			17					**42**		
Cloud LW	6	10	3	5	**3**	**4**	**8**	**14**	**12**	**8**

Table 7: Values of geopotential, wind speed, relative humidity and cloud forcing long-wave flux for periods in May and October with below average (normal text) and above average (bold script) seeing conditions. Gray shading highlights the best-case and worst-case scenarios discussed in detail in the previous sections of the text.

It is seen in this Table that there are indeed systematic differences between periods with good seeing conditions and poorer seeing conditions. The height of the 700 hPa geopotential is generally lower under conditions of less than average seeing by up to 20 m (see for example October 1997 vs. October 1989), which represents a significant contraction of the atmosphere between the ground surface and the 700 hPa geopotential level. Wind velocities are on average

higher during periods of less than average visibility, but more significantly, relative humidity and the associated cloud longwave radiative forcing are considerably higher, for the reasons evoked above.

In order to emphasize some of these points, Figure 26 illustrates the height of the 700 hPa geopotential for the Paranal area in October 1999, which is within the La Niña phase and is consequently associated with poorer seeing conditions (the seeing parameter for this particular month is 2σ higher than the average value of the seeing parameter at Paranal). The characteristic NW flow penetrating the coastal ranges of northern Chile from the Pacific is clearly seen in this figure, and closely resembles the geopotential height distribution in the examples provided in Figure 12, for the worst-case seeing scenarios. In Figure 27, the cloud forcing net longwave flux is seen to be relatively high (12 W/m^2), with the pattern of CFNLF characteristically similar to the worse-case situation illustrated in Figure 11b.

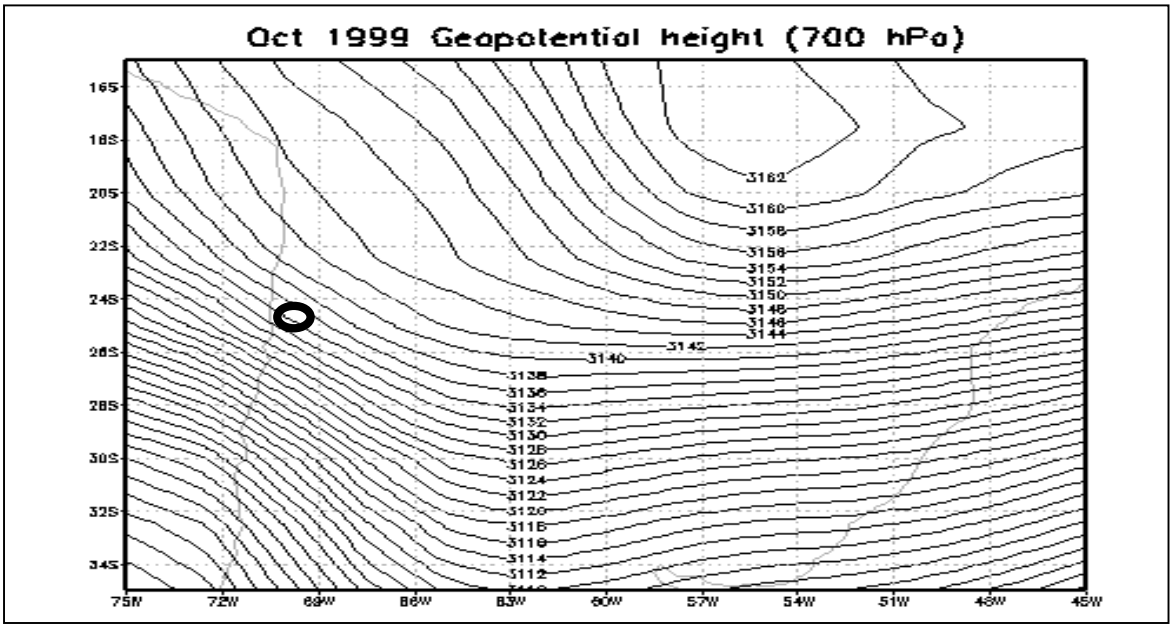

Figure 26: Geopotential field at the 700 hPa pressure surface for the central portion of Latin America, providing details on the geopotential distribution over the Paranal area for October 1999. The circle is centered on the ESO Paranal site.

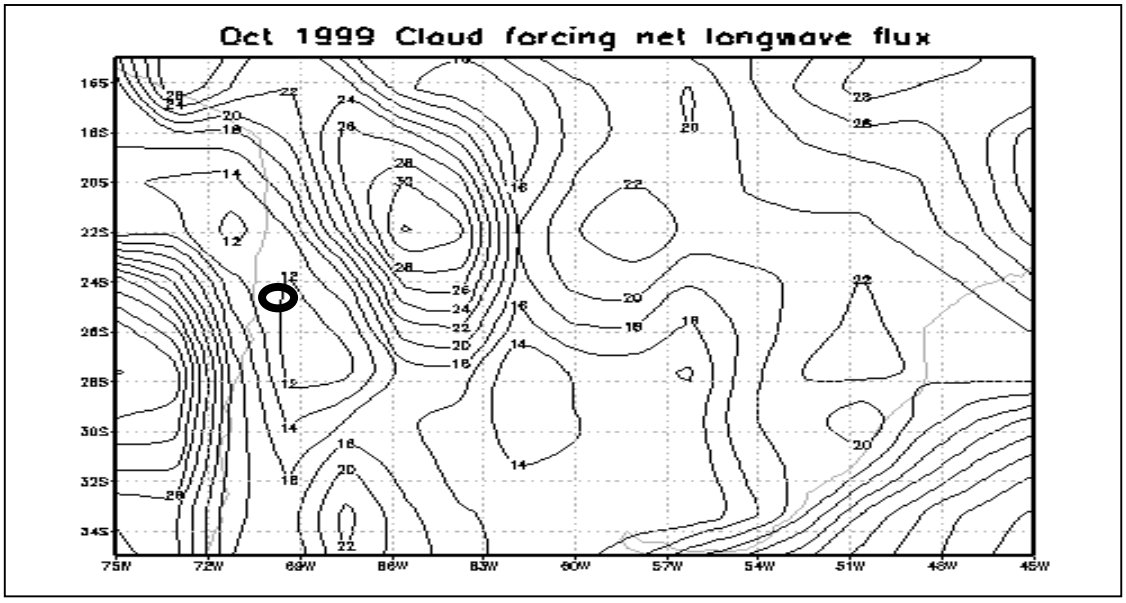

Figure 27: Cloud forcing net longwave fluxes for the central portion of Latin America, providing details on the CFNLF distribution over the Paranal area for October 1999. The circle is centered on the ESO Paranal site.

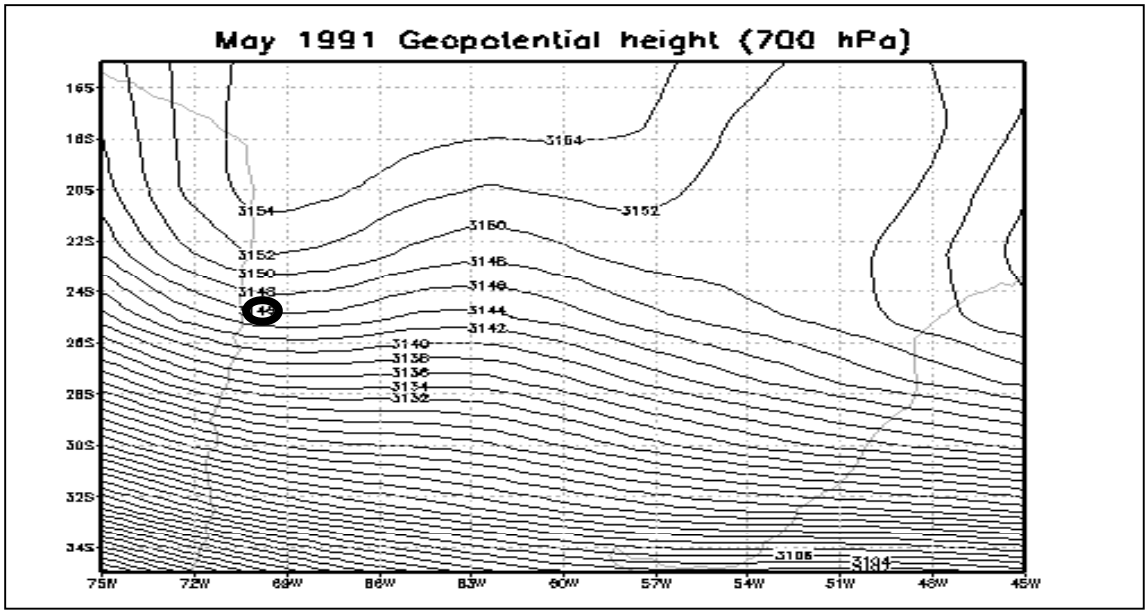

Figure 28: Geopotential field at the 700 hPa pressure surface for the central portion of Latin America, providing details on the geopotential distribution over the Paranal area for May 1991. The circle is centered on the ESO Paranal site.

At the other end of the seeing spectrum, Figures 28 and 29 show the 700 hPa geopotential field and CFNLF, respectively, for May 1991, which is 1.5σ lower than the long-term average of the seeing parameter and corresponds to optimal visibility for astronomic observations. As in the corresponding figures for the best-case scenario (Figures 15a and 23a), it is seen that the flow field

is essentially from a westerly sector and transits rapidly from the Pacific coast to the Paranal area. The high elevation of the 700 hPa level is indicative of a vertical expansion of the atmospheric column between the surface and the 700 hPa pressure surface. Concerning the CFNLF, it is seen here to be relatively low (less than 7 W/m^2), which is similar to the values of the best-case scenario illustrated in Figure 23a.

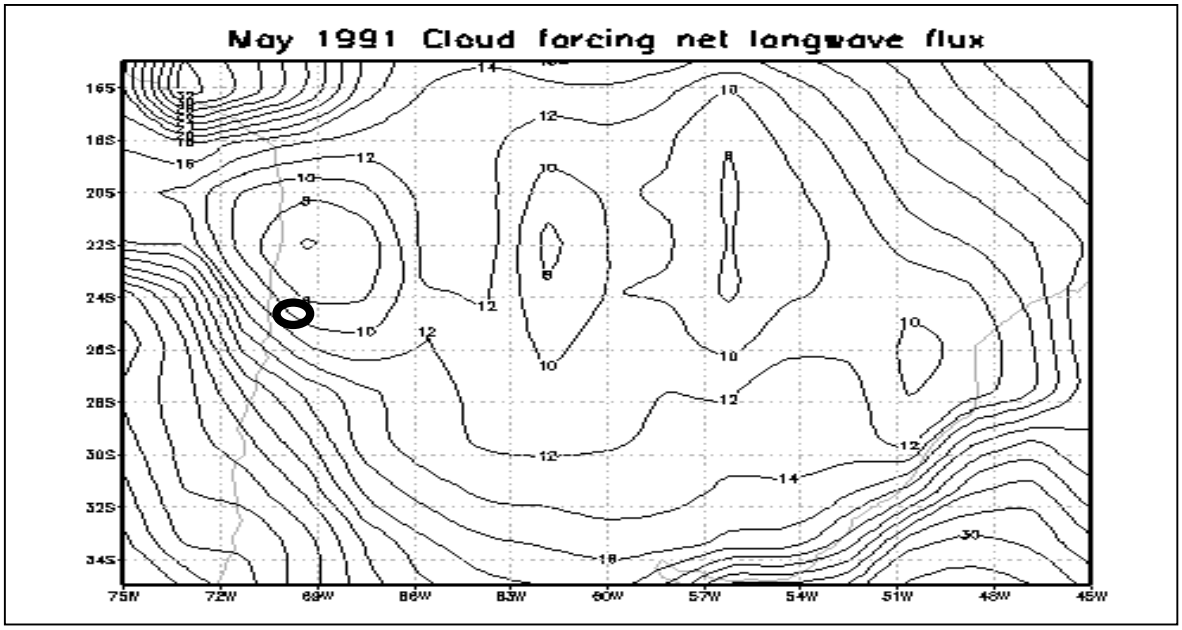

Figure 29: Cloud forcing net longwave fluxes for the central portion of Latin America, providing details on the CFNLF distribution over the Paranal area for May 1991. The circle is centered on the ESO Paranal site.

Outside of the range of instrumental observations at Paranal, a survey has been made to assess whether similar synoptic situations leading to poor seeing conditions have been observed over the last 50 years. This has been achieved by analyzing the similarities in the distribution of geopotential height (700 hPa), wind velocity, relative humidity, and cloud forcing net longwave flux since 1948 (when digitized information is available for the NCEP/NCAR datasets), compared to the worst-case scenarios discussed here (October 1998, October 1999). The assessment has shown that the following years exhibit conditions similar to the worst-case scenarios (October months): 1949, 1953, 1955, 1958, 1964, 1974, 1981, and 1990. Many, but not all, of these years are associated with La Niña events. Similar conditions to October 1998 or October 1999 can also be generated exceptionally in the absence of ENSO forcing by particular configurations of the surface pressure fields and middle and upper troposphere flows, which can result in significant moisture convergence over the Paranal area.

Two events from the above set are illustrated in the following, namely the synoptic situations of October 1958 and October 1990, in order to emphasize the fact that there have been other periods in the past with similar climatic characteristics to the 1998-2000 situation. In this sense, these most recent years are not an exceptional feature in northern Chile, even if they significantly affect optimal seeing conditions.

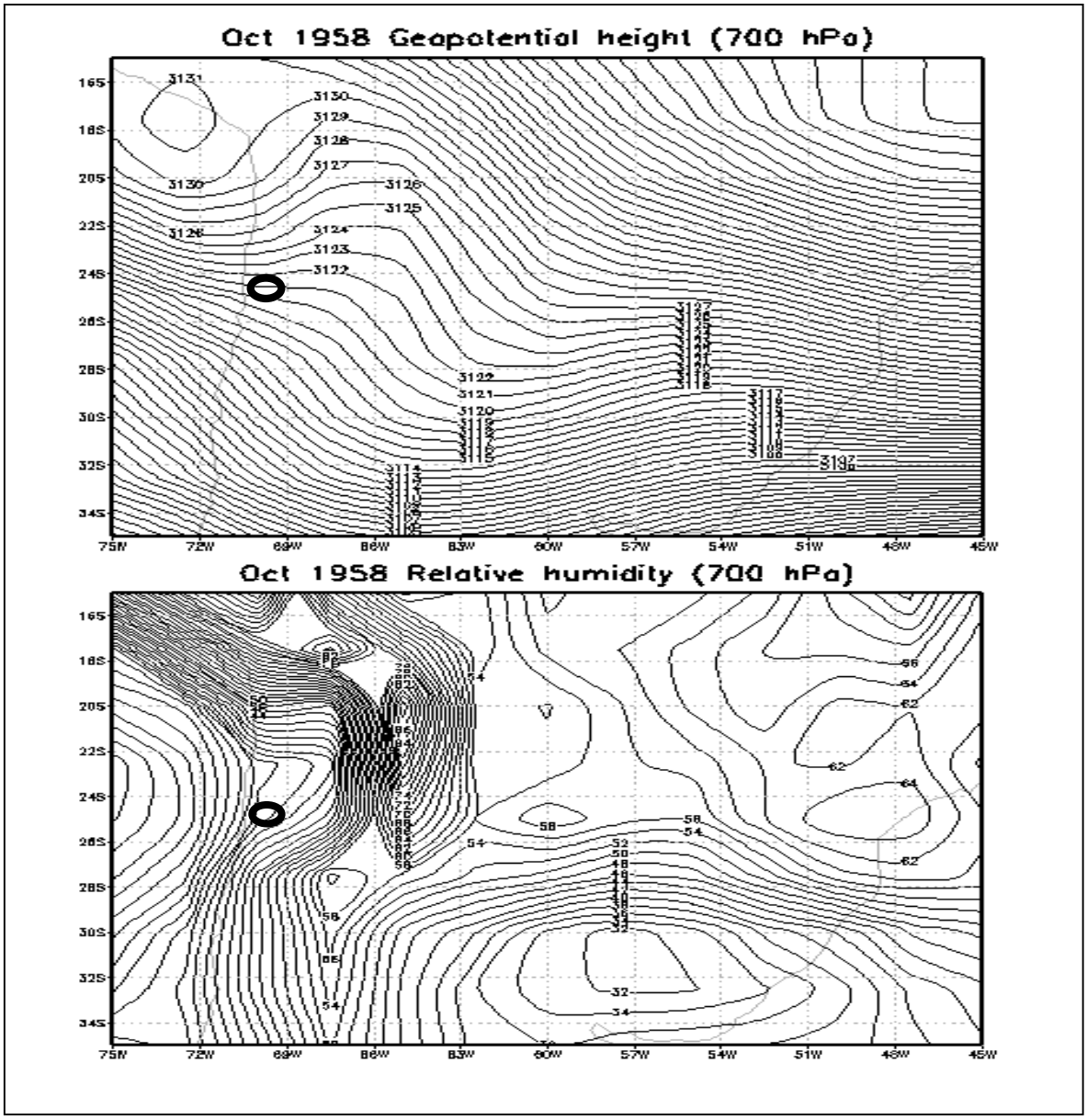

Figure 30: Synoptic situation over central Latin America in October 1958 for the 700 hPa values of a) geopotential height and b) relative humidity. The circle is centered on the ESO Paranal site.

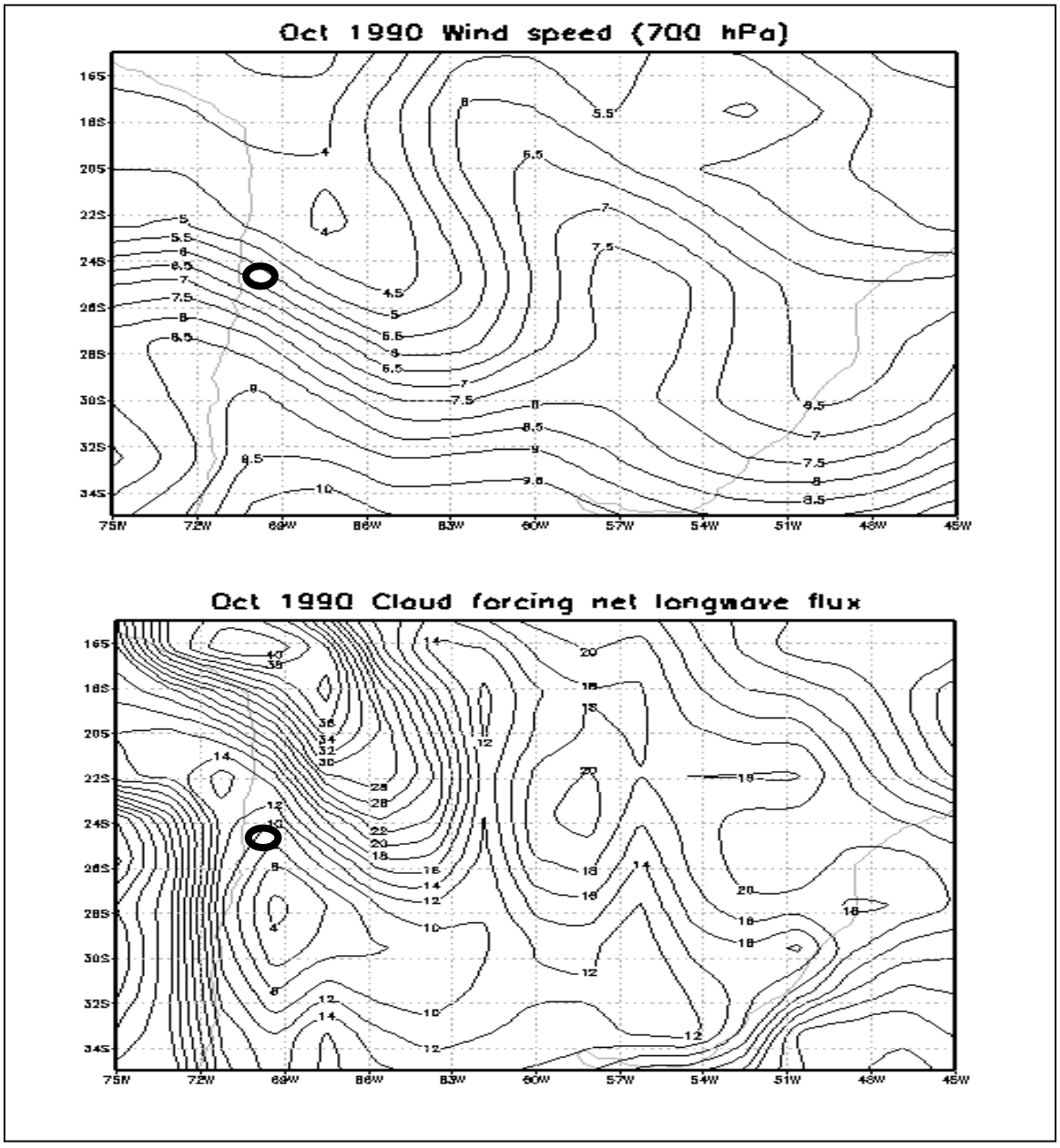

Figure 31: Synoptic situation over central Latin America in October 1990 for the 700 hPa wind velocity (above) and cloud forcing net longwave flux (below) . The circle is centered on the ESO Paranal site.

The salient features already seen in the detailed analyses of the May and October 1998 synoptic charts are well reproduced here, namely the north-westerly flow along the 700 hPa geopotential isolines, high relative humidity, stronger winds and enhanced cloud forcing net longwave radiation, are replicated in Figures 30 and 31 for earlier periods in the 20th Century.

It can thus be concluded from these selected examples, and from further analyses of other periods of good and bad seeing conditions not shown here, that there are systematic differences which are

seen to occur between periods where seeing is either favorable or poor. The most obvious difference is related to the changes in moisture content of the atmosphere which, if small compared to equatorial or mid-latitude zones, nonetheless seems to play a key role in determining conditions of astronomic observation at Paranal.

6. Conclusions

The principal conclusions of this study may thus be summarized as follows:

- The somewhat disappointing conditions for optimal astronomic observations that have prevailed since 1998 at the ESO VLT Paranal site are apparently not the result of a long-term trend in climate, related to global warming.
- The Paranal site is highly sensitive to ENSO forcing, despite its altitude and the fact that it lies well above the maritime boundary layer.
- The less than average seeing conditions are related to the onset of La Niña events. Atmospheric circulation changes and, especially, moisture convergence in the Paranal area, which are a regional consequence of the presence of the cold phase of ENSO, seem to be the most likely cause for a reduction in the seeing potential of the VLT.
- The presence of enhanced atmospheric moisture during La Niña events is potentially capable of increasing high-level cloudiness. Even thin cirrus-type clouds are be capable of perturbing the quality of astronomical observations by the VLT.
- While increased moisture and/or cloudiness account for 55% of the variance in seeing conditions, additional factors leading to a reduction in seeing may be related to the particular orientation of the flows during La Niña conditions. These tend to enhance turbulence, which in turn perturbs the thermal stratification of the atmosphere, and hence poorer seeing conditions.
- The lower than average seeing conditions experienced in 1998-2000 are not a unique event in the history of the Paranal site. By using the Antofagasta climatological record as a proxy, it is seen that other periods in the past (for example in 1958 and 1990) have exhibited similar behavior in 700 hPa airflows, wind velocities, and moisture content of the atmosphere. Had the VLT been operational at that time, astronomical observations would have been equally disrupted as during 1998 and subsequent years.
- However, the particular severity of the 1998 La Niña event explains to a large extent the sequence of unfavorable seeing conditions, which are not quite as clearly replicated as elsewhere in the existing record, because no signal is as strong in the 20th Century as the 1998-2000 La Niña.

- Until predictions of ENSO events are improved, there is for the moment no certainty as to whether poor seeing conditions will recur, and with which frequency.

7. Acknowledgements

The authors would like to warmly thank Dr. Marc Sarazin (ESO, Garching, Germany) for his time and patience in answering their numerous questions. Thanks also to Dr. Stéphane Goyette for his advice on data handling and analysis, as well as his assistance with operating the GrADS software package.

The authors acknowledge the valuable contributions, through the datasets which they have made available for this study, Dr. John Eischeid (NOAA-CDC in Boulder, Colorado: time-series of temperature at Antofagasta) and Cpt. Rodrigo Núñez G. (Servicio Hidrólogico y Oceanográfico de Chile – SHOA: superficial ocean temperature time series off Antofagasta).

The NCEP Reanalysis data is provided by the NOAA-CIRES Climate Diagnostics Center, Boulder, Colorado, USA, from their Web site at http://www.cdc.noaa.gov/ for the 2-dimensional surface plots of geopotential height, relative humidity, cloud forcing net longwave flux, wind speed and sea surface temperature. The public availability of data (Southern Oscillation Index) from the Climate and Global Dynamics Division of the University Corporation for Atmospheric Research (UCAR/CGD on URL: http://www.cgd.ucar.edu/cas/catalog/climind/soi.html) and the software package GrADS from the Center for Ocean-Land-Atmosphere Studies (COLA on URL: http://grads.iges.org/grads/) are gratefully acknowledged.

This study has been undertaken under contract with the European Southern Observatory (ESO) contract number: 61243 / ODG / 00 / 8543 / GWI / LET .

8. References

8.1 Publications

Bustos, R., 2000: A 52-Year Climatological Study for the Paranal Area Using NCEP/NCAR Reanalysis Data

Erasmus, D. A., 1998: The effects of El Niño - Southern Oscillation on the seasonal, inter-annual and spatial variability of water vapour and cirrus cloud cover over Northern Chile. A Satellite-Derived Climatology of Water Vapour and Cirrus Cloud Cover in the Area of Chajnantor, Northern Chile.
http://www.eso.org/gen-fac/pubs/astclim/espas/radioseeing/erasmus/proposal1.htm

Jones, P.D., New, M., Parker, D.E., Martin, S. and Rigor, I.G., 1999 : Surface air temperature and its changes over the past 150 years. Reviews of Geophysics, 37, 173-199

Romero, H., 1985: Geografía de los climas de Chile. Instituto Geográfico Militar, 142-158

Wolter K., and M.S. Timlin, 1998: Measuring the strength of ENSO events - how does 1997/98 rank? Weather**,** 53**,** 220-242

8.2 Internet sites

http://www.assa.org.au/observing/seeing

http://www.cdc.noaa.gov

http://www.cgd.ucar.edu/cas/catalog/climind/soi.html

http://www.dgf.uchile.cl/

http://www.eso.org

http://grads.iges.org/grads/